mRNA vaccine-elicited antibodies to SARS-CoV-2 and circulating variants

Zijun Wang[1,*], Fabian Schmidt[2,*], Yiska Weisblum[2,*], Frauke Muecksch[2,*], Christopher O. Barnes[3,*], Shlomo Finkin[1,*], Dennis Schaefer-Babajew[1,*], Melissa Cipolla[1*], Christian Gaebler[1*], Jenna A. Lieberman[4,*], Zhi Yang[3], Morgan E. Abernathy[3], Kathryn E. Huey-Tubman[3], Arlene Hurley[5], Martina Turroja[1], Kamille A. West[6], Kristie Gordon[1], Katrina G. Millard[1], Victor Ramos[1], Justin Da Silva[2], Jianliang Xu[4], Robert A. Colbert[7], Roshni Patel[1], Juan Dizon[1], Cecille Unson-O'Brien[1], Irina Shimeliovich[1], Anna Gazumyan[1], Marina Caskey[1], Pamela J. Bjorkman[3,#], Rafael Casellas[4,8,#], Theodora Hatziioannou[2,#], Paul D. Bieniasz[2,9,#], Michel C. Nussenzweig[1,9,#]

[1]Laboratory of Molecular Immunology, The Rockefeller University, New York, NY 10065, USA.

[2]Laboratory of Retrovirology, The Rockefeller University, New York, NY 10065, USA.

[3] Division of Biology and Biological Engineering, California Institute of Technology, Pasadena, CA, USA.

[4]Lymphocyte Nuclear Biology, National Institute of Arthritis and Musculoskeletal and Skin Diseases, National Institutes of Health, Bethesda, MD 20892.

[5]Hospital Program Direction, The Rockefeller University, New York, NY 10065, USA.

[6]Department of Transfusion Medicine, National Institutes of Health Clinical Center, Bethesda, MD 20892.

[7]Pediatric Translational Research Branch and Office of the Clinical Director, National Institute of Arthritis and Musculoskeletal and Skin Diseases, National Institutes of Health, Bethesda, MD 20892.

[8]The NIH Regulome Project, National Institutes of Health, Bethesda, MD 20892.

[9] Howard Hughes Medical Institute

[*]Equal contribution

[#]Send correspondence to Paul Bieniasz: pbieniasz@rockefeller.edu; Pamela Bjorkman: bjorkman@caltech.edu; Rafael Casellas: rafael.casellas@nih,gov; Theodora Hatziioannou: thatziio@rockefeller.edu; Michel C. Nussenzweig: nussen@rockefeller.edu

To date severe acute respiratory syndrome coronavirus-2 (SARS-CoV-2) has infected nearly 100 million individuals resulting in over two million deaths. Many vaccines are being deployed to prevent coronavirus disease-2019 (COVID-19) including two novel mRNA-based vaccines[1,2]. These vaccines elicit neutralizing antibodies and appear to be safe and effective, but the precise nature of the elicited antibodies is not known[3-5]. Here we report on the antibody and memory B cell responses in a cohort of 20 volunteers who received either the Moderna (mRNA-1273) or Pfizer-BioNTech (BNT162b2) vaccines. Consistent with prior reports, 8 weeks after the second vaccine injection volunteers showed high levels of IgM, and IgG anti-SARS-CoV-2 spike protein (S), receptor binding domain (RBD) binding titers[3,5]. Moreover, the plasma neutralizing activity, and the relative numbers of RBD-specific memory B cells were equivalent to individuals who recovered from natural infection[6,7]. However, activity against SARS-CoV-2 variants encoding E484K or N501Y or the K417N:E484K:N501Y combination was reduced by a small but significant margin. Consistent with these findings, vaccine-elicited monoclonal antibodies (mAbs) potently neutralize SARS-CoV-2, targeting a number of different RBD epitopes epitopes in common with mAbs isolated from infected donors. Structural analyses of mAbs complexed with S trimer suggest that vaccine- and virus-encoded S adopts similar conformations to induce equivalent anti-RBD antibodies. However, neutralization by 14 of the 17 most potent mAbs tested was reduced or abolished by either K417N, or E484K, or N501Y mutations. Notably, the same mutations were selected when recombinant vesicular stomatitis virus (rVSV)/SARS-CoV-2 S was cultured in the presence of the vaccine elicited mAbs. Taken together the results suggest that the monoclonal antibodies in clinical use

should be tested against newly arising variants, and that mRNA vaccines may need to be updated periodically to avoid potential loss of clinical efficacy.

Between 19 October 2020 and 15 January 2021, 20 volunteers who received two doses of the Moderna (n=14) or Pfizer-BioNTech mRNA (n=6) vaccines were recruited for blood donation and analyzed. Ages of the analyzed volunteers ranged from 29-69 years (median 43); 12 (60%) were male and 8 (40%) female. 16 participants identified as Caucasian, 2 as Hispanic, and 1 as African American or Asian, respectively. The time from the second vaccination to sample collection varied between 3-14 weeks with an average of 8 weeks. None of the volunteers had a history of prior SARS-CoV-2 infection and none experienced serious adverse events after vaccination (Extended Data Table 1).

Vaccinee plasma binding and neutralizing activity against SARS-CoV-2

Plasma IgM and IgG anti-SARS-CoV-2 S and RBD were measured by enzyme-linked immunosorbent assay (ELISA)[6,7]. All individuals tested showed reactivity to S and RBD that was significantly higher compared to pre-COVID-19 historic controls (Extended Data Fig 1). As might be expected anti-S and -RBD IgG levels were higher than IgM or IgA. Moreover, there was greater variability in the anti-RBD than the anti-S response but the two were positively correlated (Extended Data Fig 1).

Plasma neutralizing activity was determined using HIV-1 pseudotyped with SARS-CoV-2 S protein[6-8]. In agreement with previous reports, there was a broad range of plasma neutralizing activity 3-14 weeks after the second vaccine dose that was similar to that elicited by natural infection in a convalescent cohort after 1.3 months, and greater than the activity at 6.2 months after infection (Fig. 1a, Extended Data Table 1). There was no significant difference in neutralizing activity between the Moderna and Pfizer-BioNTech vaccines (Fig. 1b). As

expected, plasma neutralizing activity was directly correlated to anti-S and -RBD binding titers in ELISAs[6,7] (Fig. 1c, d, and Extended Data Fig. 2a-d). Finally, RBD and S binding, and neutralizing activities were directly correlated to the time between the first vaccine dose and blood donation with significantly reduced levels in all 3 measurements with time (Fig. 1e-g, and Extended Data Fig. 2e-h)[9].

To determine whether plasma from vaccinated individuals can neutralize circulating SARS-CoV-2 variants of concern and mutants that arise *in vitro* under antibody pressure [10,11], we tested vaccinee plasma against a panel of 10 mutant pseudotype viruses including recently reported N501Y (B1.1.7 variant), K417N, E484K and the combination of these 3 RBD mutations (501Y.V2 variant)[12-17]. Vaccinee plasma was significantly less effective in neutralizing the HIV-1 virus pseudotyped with certain SARS-CoV-2 mutant S proteins (Fig. 1h and i and Extended Data Fig. 2j). Among the volunteer plasmas tested there was an 1 to 3, 1.3 to 2.5, and 1.1 to 3 fold decrease in neutralizing activity against E484K, N501Y and the K417N:E484K:N501Y combination respectively ($p= 0.0033$, $p=0.0002$, and $p<0.0001$, respectively, Fig. 1h and i). We conclude that the plasma neutralizing activity elicited by mRNA vaccination is variably but significantly less effective against particular RBD mutants in the tested panel.

Vaccine-elicited SARS-CoV-2 RBD-specific monoclonal antibodies

Although circulating antibodies derived from plasma cells wane over time, long-lived immune memory can persist in expanded clones of memory B cells[6]. We used flow cytometry to enumerate the circulating SARS-CoV-2 RBD-specific memory B cells elicited by mRNA immunization[6,7] (Fig. 2a, Extended Data Fig. 3a and b). Notably, the percentage of RBD-binding

memory B cells in vaccinees was significantly greater than in naturally infected individuals assayed after 1.3 months, but similar to the same individuals assayed after 6.2 months (Fig. 2b). The percentage of RBD-binding memory B cells in vaccinees was not correlated to the time after vaccination (Extended Data Fig. 3c). Thus, mRNA vaccination elicits a robust SARS-CoV-2 RBD-specific B cell memory response that resembles natural infection.

To examine the nature of the antibodies produced by memory B cells in response to vaccination, we obtained 1,409 paired antibody heavy and light chains from RBD binding single B cells from 14 individuals (n=10 Moderna and n=4 Pfizer-BioNTech vaccinees) (Extended Data Table 2). Expanded clones of cells comprised 4-50% of the overall RBD binding memory B cell compartment (Fig. 2c and d, and Extended Data Fig. 3d). Similar to natural infection, IGVH 3-53, and 3-30 and some IGVL genes were significantly over-represented in the RBD-binding memory B cell compartment of vaccinated individuals (Fig. 2e, Extended Data Fig. 4a). In addition, antibodies that share the same combination of IGHV and IGLV genes in vaccinees comprised 39% of all the clonal sequences (Extended Data Fig. 4b) and 59% when combined with naturally infected individuals[6,7] (Fig. 2f), and some of these antibodies were nearly identical (Extended Data Table 2 and 3). The number of V gene nucleotide mutations in vaccinees is greater than in naturally infected individuals assayed after 1.3 months, but lower than that in the same individuals assayed after 6.2 months (Fig. 2g and Extended Data Fig. 5a). The length of the IgH CDR3 was similar in both natural infected individuals and vaccinees and hydrophobicity was below average[18] (Fig. 2h and Extended Data Fig. 5a and b). Thus, the IgG memory response is similar in individuals receiving the Pfizer-BioNTech and Moderna vaccines and both are rich in recurrent and clonally expanded antibody sequences.

Eighty-four representative antibodies from 4 individuals were expressed and tested for reactivity to the RBD (Extended Data Table 4). The antibodies included: (1) 58 that were randomly selected from those that appeared only once, and (2) 26 representatives of expanded clones. Of the antibodies tested 99% (83 out of the 84) bound to RBD indicating that single cell sorting by flow cytometry efficiently identified B cells producing anti-RBD antibodies (Extended Data Fig. 6a and b and Table 4). In anti-RBD ELISAs the mean half-maximal effective concentration (EC_{50}) was higher than that observed in infected individuals after 6 months but not significantly different from antibodies obtained 1.3 months after infection (Extended Data Fig. 6a, and Table 4 and [6,7]). To examine memory B cell antibodies for binding to circulating SARS-CoV-2 variants and antibody resistant mutants we performed ELISA assays using mutant RBDs[10,13,19-22]. Twenty-two (26%) of the antibodies showed at least 5-fold decreased binding to at least one of the mutant RBDs (Extended data Fig. 6c-l, and Table 4).

SARS-CoV-2 S pseudotyped viruses were used to measure the neutralizing activity of all 84 antibodies[6-8] (Fig. 3a, Extended Data Table 4). Consistent with the plasma neutralization results, the geometric mean neutralization half-maximal inhibitory concentration of the vaccinee antibodies (IC_{50}=151 ng/ml) was not significantly different to antibody collections obtained from naturally infected individuals 1.3 or 6.2 months after infection (Fig. 3a and [6,7]).

To examine the neutralizing breadth of the monoclonal antibodies and begin to map their target epitopes we tested the 17 most potent antibodies (Extended data Table 5), 8 of which carried IgHV3-53, against a panel of 12 SARS-CoV-2 variants: A475V is resistant to class 1 antibodies

(structurally defined as described[20]); E484K and Q493R are resistant to class 2 antibodies[6,7,10,11,20,21,23,24]; while R346S, N439K, and N440K are resistant to class 3 antibodies[6,7,10,11,20,24]. Additionally, K417N, Y453F, S477R, N501Y, D614G, and R683G represent circulating variants some of which have been associated with rapidly increasing case numbers[12,13,24-27]. Based on their neutralizing activity against the variants, all but 3 of the antibodies were provisionally assigned to a defined antibody class or a combination (Fig. 3b). As seen in natural infection, a majority of the antibodies tested (9/17) were at least ten-fold less effective against pseudotyped viruses carrying the E484K mutation[6,10,20]. In addition, 5 of the antibodies were less potent against K417N and 4 against N501Y by ten-fold or more (Fig. 3b).

To determine whether antibody-imposed selection pressure could also drive the emergence of resistance mutations *in vitro,* we cultured an rVSV/SARS-CoV-2 recombinant virus in the presence of each of 18 neutralizing monoclonal antibodies. All of the tested antibodies selected for RBD mutations. Moreover, in all cases the selected mutations corresponded to residues in the binding sites of their presumptive antibody class (Fig. 3b and c). For example, antibody 627, which was assigned to class 2 based on sensitivity to E484K mutation, selected for the emergence of the E484K mutation *in vitro* (Fig 3c). Notably, 6 of the antibodies selected for K417N E or T, 5 selected for E484K and 3 selected for N501Y, T or H, which coincide with mutations present in the circulating B1.1.17, 501Y.V2 and B1.1.28/501.V3 variants that have been associated with rapidly increasing case numbers in particular locales[12,15,17,28].

Cryo-EM mapping of antibody epitopes

To further characterize antibody epitopes and mechanisms of neutralization, we characterized seven complexes between mAb Fab fragments and the prefusion, stabilized ectodomain trimer of SARS-CoV-2 S glycoprotein[29] using single-particle cryo-EM (Fig. 4 and Extended Data Table 6). Overall resolutions ranged from 5-8 Å and coordinates from S trimer and representative Fab crystal structures were fit by rigid body docking into the cryo-EM density maps to provide a general assessment of antibody footprints/RBD epitopes. Fab-S complexes exhibited multiple RBD-binding orientations recognizing either 'up'/'down' (Fig. 4a-j) or solely 'up' (Fig. 4k-n) RBD conformations, consistent with structurally defined antibody classes from natural infection (Fig. 4o)[20]. The majority of mAbs characterized (6 of 7) recognized epitopes that included RBD residues involved in ACE2 recognition, suggesting a neutralization mechanism that directly blocks ACE2-RBD interactions. Additionally, structurally defined antibody epitopes were consistent with RBD positions that were selected in rVSV/SARS-CoV-2 recombinant virus outgrowth experiments, including residues K417, N439/N440, E484, and N501 (Fig. 3c and Fig. 4f-j,m,n). Taken together, these data suggest that functionally similar antibodies are raised during vaccination and natural infection, and that the RBDs of spike trimers translated from the mRNA delivered by vaccination adopt a similar distribution of 'up'/'down' conformations as observed on SARS-CoV-2 virions.

Discussion

The mRNA-based SARS-CoV-2 vaccines are safe and effective and being deployed globally to prevent infection and disease. The vaccines elicit antibody responses against the RBD, the major target of neutralizing antibodies[30-35], in a manner that resembles natural infection. Notably, the neutralizing antibodies produced by mRNA vaccination target the same epitopes as natural

196 infection. The data is consistent with SARS-CoV-2 spike trimers translated from the injected
197 RNA adopting the range of conformations available to spikes on the surfaces of virions.
198 Moreover, different individuals immunized with either the Moderna (mRNA-1273) or Pfizer-
199 BioNTech (BNT162b2) vaccines produce closely related and nearly identical antibodies.
200
201 Human neutralizing monoclonal antibodies to the SARS-CoV-2 RBD can be categorized as
202 belonging to 4 different classes based on their target regions on the RBD[20]. Class 1 and 2
203 antibodies are among the most potent and also the most abundant antibodies[6,7,30,31,34]. These
204 antibodies target epitopes that overlap or are closely associated with RBD residues K417, E484
205 and N501. They are frequently sensitive to mutation in these residues and select for K417N,
206 E484K and N501Y mutations in both yeast and VSV expressing SARS-CoV-2 S proteins[10,13,24].
207 To avert selection and escape, antibody therapies should be composed of combinations of
208 antibodies that target non-overlapping epitopes[7,10,11,24,36-38].
209
210 A number of circulating SARS-CoV-2 variants that have been associated with rapidly increasing
211 case numbers and have particular prevalence in the UK (B1.1.7/501Y.V1), South Africa
212 (501Y.V2) and Brazil (B1.1.28/501.V3)[12,15,17,28,39]. Our experiments indicate that these variants,
213 and potentially others that carry K417N/T, E484K and N501Y mutations, can reduce the
214 neutralization potency of vaccinee plasma. The comparatively modest effects of the mutations on
215 viral sensitivity to plasma reflects the polyclonal nature of the neutralizing antibodies in vaccinee
216 plasma. Nevertheless, emergence of these particular variants is consistent with the dominance of
217 the class 1 and 2 antibody response in infected or vaccinated individuals and raises the
218 possibility that they emerged in response to immune selection in individuals with non-sterilizing

219 immunity. What the long-term effect of accumulation of mutations on the SARS-CoV-2
220 pandemic will be is not known, but the common cold coronavirus HCoV-229E evolves antigenic
221 variants that are comparatively resistant to the older sera but remain sensitive to
222 contemporaneous sera[40]. Thus, it is possible that these mutations and others that emerge in
223 individuals with suboptimal or waning immunity will erode the effectiveness of natural and
224 vaccine elicited immunity. The data suggests that SARS-CoV-2 vaccines may need to be updated
225 and immunity monitored in order to compensate for viral evolution.
226

Figure Legends

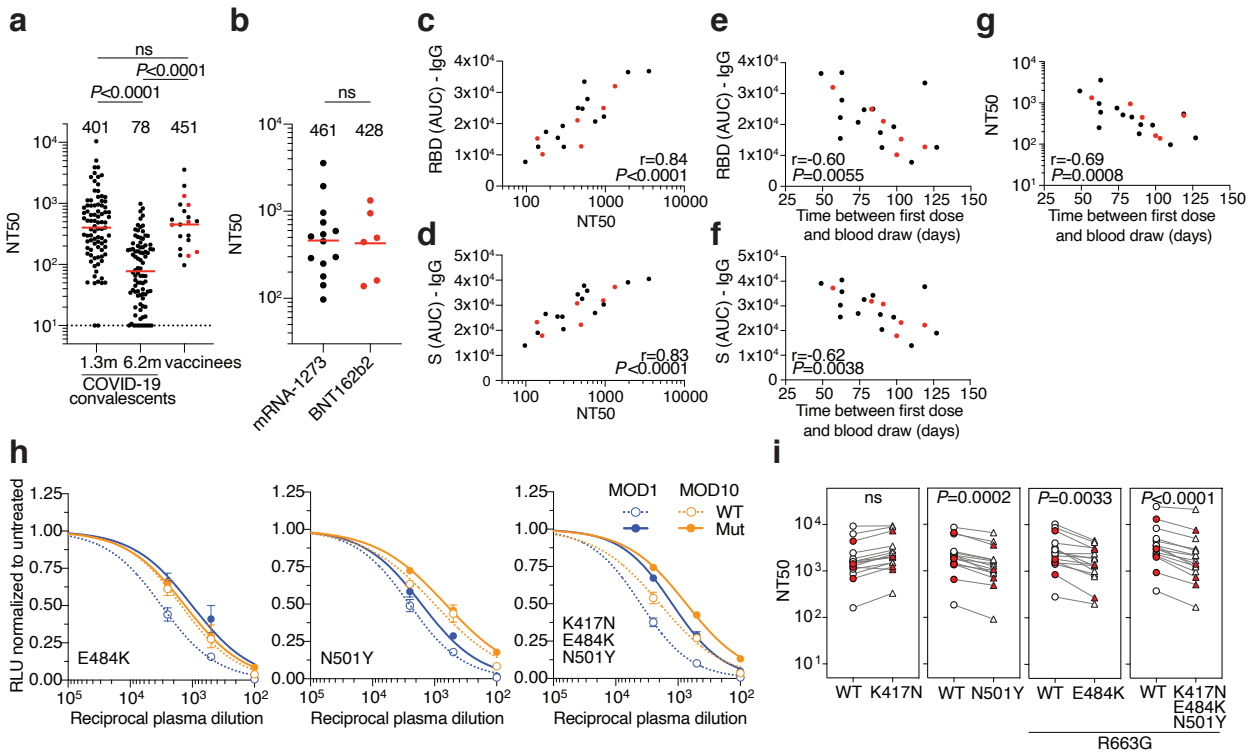

Fig. 1. Plasma neutralizing activity. a, SARS-CoV-2 pseudovirus neutralization assay. NT_{50} values for COVID-19 convalescent plasma measured at 1.3 months[7] and 6.2 months[6] as well as plasma from mRNA-vaccinees. NT_{50} values lower than 10 were plotted at 10. Mean of 2 independent experiments. Red bars and indicated values represent geometric mean NT_{50} values. Statistical significance was determined using the two-tailed Mann-Whitney U-test. **b**, NT_{50} values for Moderna (black) and Pfizer-BioNTech (red) vaccine recipients. Red bars and indicated values represent geometric mean NT_{50} values. Statistical significance was determined using the two-tailed Mann-Whitney U-test. **c**, Anti-RBD IgG AUC (Y axis) plotted against NT_{50} (X axis) r=0.84, p<0.0001. **d,** Anti-S IgG AUC (Y axis) plotted against NT_{50} (X axis) r=0.83, p<0.0001. **e**, Anti-RBD IgG AUC (Y axis) plotted against time between first dose and blood draw (X axis) r=-0.60 p=0.0055. **f**, Anti-S IgG AUC (Y axis) plotted against time between first

dose and blood draw (X axis) r=-0.62 p=0.0038. **g**, NT_{50} (Y axis) plotted against time between first dose and blood draw (X axis) r=-0.69 p=0.0008. The r and p values for correlations in **c-g** were determined by two-tailed Spearman correlation. Moderna vaccinees are in black and Pfizer-BioNTech in red. **h.** Examples of neutralization assays, comparing the sensitivity of pseudotyped viruses with WT and RBD mutant SARS-CoV-2 S proteins to vaccinee plasma. **i,** NT50 values for vaccinee plasma (n=15) neutralization of pseudotyped viruses with WT and the indicated RBD-mutant SARS-CoV-2 S proteins. Statistical significance was determined using one tailed t-test. All experiments were performed a minimum of 2 times. Pfizer-BioNTech vaccinees in red.

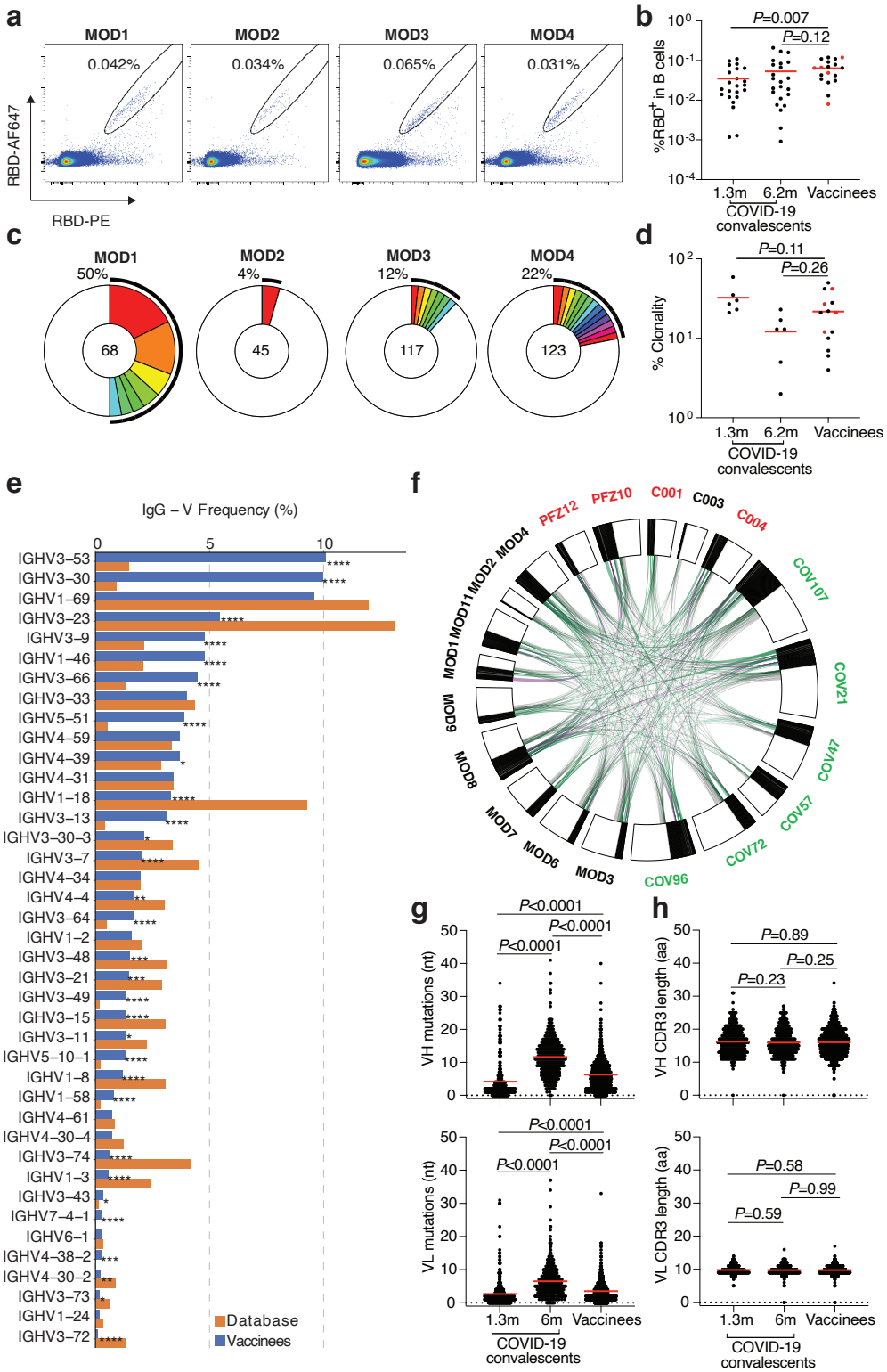

249

Fig. 2. Memory B cell antibodies. a, Representative flow cytometry plots showing dual AlexaFluor-647-RBD and PE-RBD binding B cells for 4 vaccinees. **b,** as in **a,** dot plot summarizes the percentage of RBD binding B cells in 19 vaccinees, in comparison to a cohort of infected individuals assays 1.3 and 6.2 months after infection[6,7]. Individuals who received the Moderna vaccine are shown in black and Pfizer-BioNTech vaccine recipients in red. Red horizontal bars indicate mean values. Statistical significance was determined using two-tailed Mann–Whitney U-tests. **c,** Pie charts show the distribution of antibody sequences from the 4 individuals in **a.** The number in the inner circle indicates the number of sequences analyzed. Pie slice size is proportional to the number of clonally related sequences. The black outline indicates the frequency of clonally expanded sequences. **d,** as in **c,** graph shows relative clonality among 14 vaccinees assayed, individuals who received the Moderna vaccine are shown in black and Pfizer-BioNTech vaccine recipients in red. Red horizontal bars indicate mean values. Statistical significance was determined using two-tailed Mann–Whitney U-tests. **e,** Graph shows relative abundance of human IGVH genes Sequence Read Archive accession SRP010970 (orange), and vaccinees (blue). A two-sided binomial test was used to compare the frequency distributions, significant differences are denoted with stars (* $p < 0.05$, ** $p < 0.01$, *** $p < 0.001$, **** = $p < 0.0001$). **f,** Clonal relationships between sequences from 14 vaccinated individuals (Moderna in black, Pfizer-BioNTech in red Extended Data Table 2) and naturally infected individuals (in green, from[6,7]). Interconnecting lines indicate the relationship between antibodies that share V and J gene segment sequences at both IGH and IGL. Purple, green and grey lines connect related clones, clones and singles, and singles to each other, respectively. **g,** Number of somatic nucleotide mutations in the IGVH (top) and IGVL (bottom) in vaccinee antibodies (Extended Data Table 2) compared to natural infection obtained 1.3 or 6.2 months after infection[6,7].

273 Statistical significance was determined using the two-tailed Mann–Whitney U-tests and red

274 horizontal bars indicate mean values. **h,** as in **g,** but for CDR3 length.

275

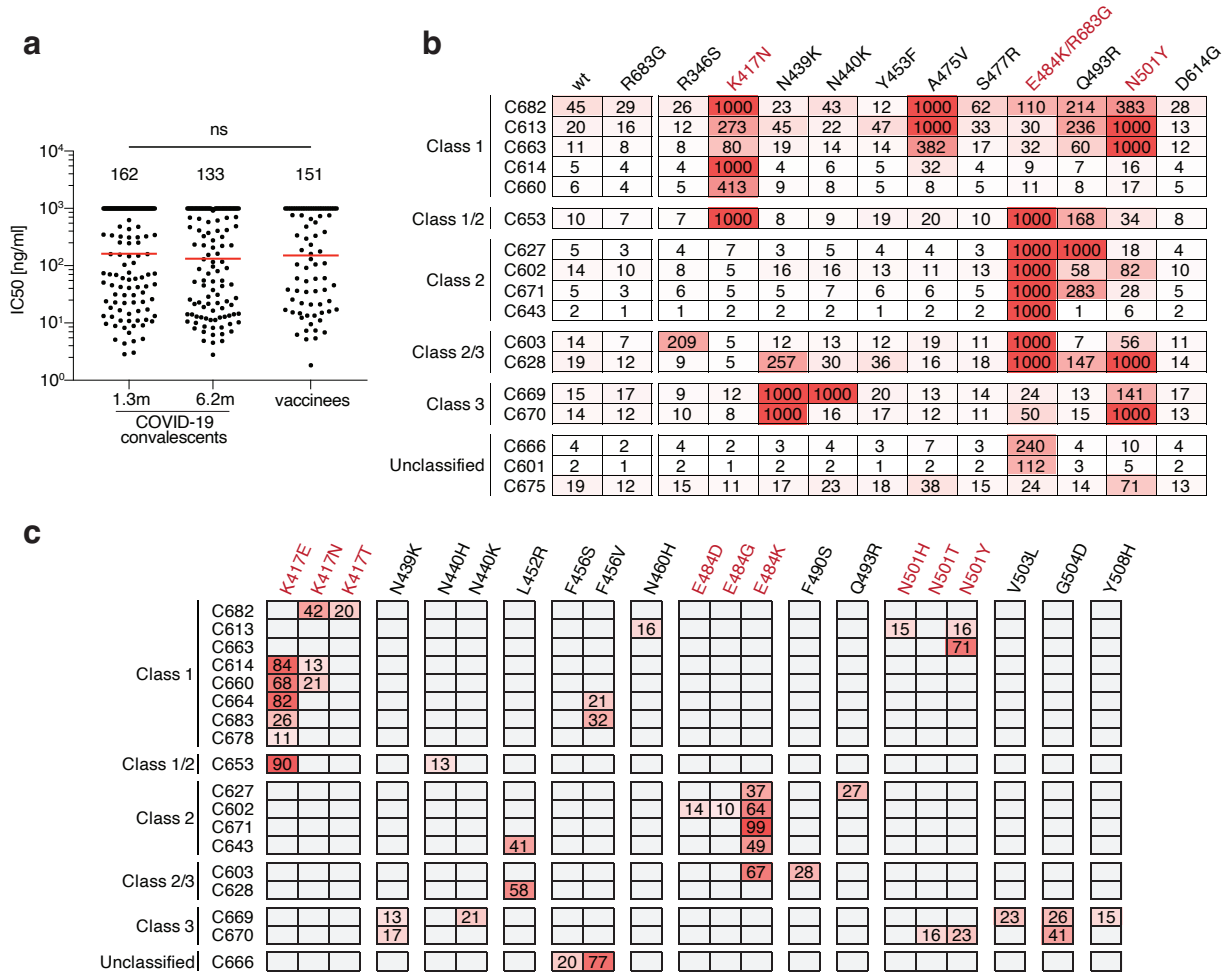

276

277 **Fig. 3: Anti-SARS-CoV-2 RBD monoclonal antibody neutralizing activity. a,** SARS-CoV-2

278 pseudovirus neutralization assay. IC_{50} values for antibodies cloned from COVID-19

279 convalescent patients measured at 1.3 and 6.2 months[6,7] as well as antibodies cloned from

280 mRNA-vaccinees. Antibodies with IC_{50} values above 1000 ng/ml were plotted at 1000 ng/ml.

281 Mean of 2 independent experiments. Red bars and indicated values represent geometric mean

282 IC_{50} values in ng/ml. Statistical significance was determined using the two-tailed Mann-Whitney

283 U-test. **b,** IC_{50} values for 17 selected mAbs for neutralization of wild type and the indicated

284 mutant SARS-CoV-2 pseudoviruses. Color gradient indicates IC_{50} values ranging from 0 (white)

285 to 1000 ng/ml (red). **c**, Antibody selection pressure can drive emergence of S variants in cell
286 culture; the percentage of sequence reads encoding the indicated RBD mutations after a single
287 passage of rVSV/SARS-CoV-2 in the presence of the indicated antibodies is tabulated. Color
288 gradient indicates percentage of sequence reads bearing the indicated mutation ranging from 0
289 (white) to 100 (red). Positions for which no sequence read was detected are shown in grey.
290 K417N, E484K/R683G and N501 are highlighted in b and c as they constitute important
291 circulating variants.
292

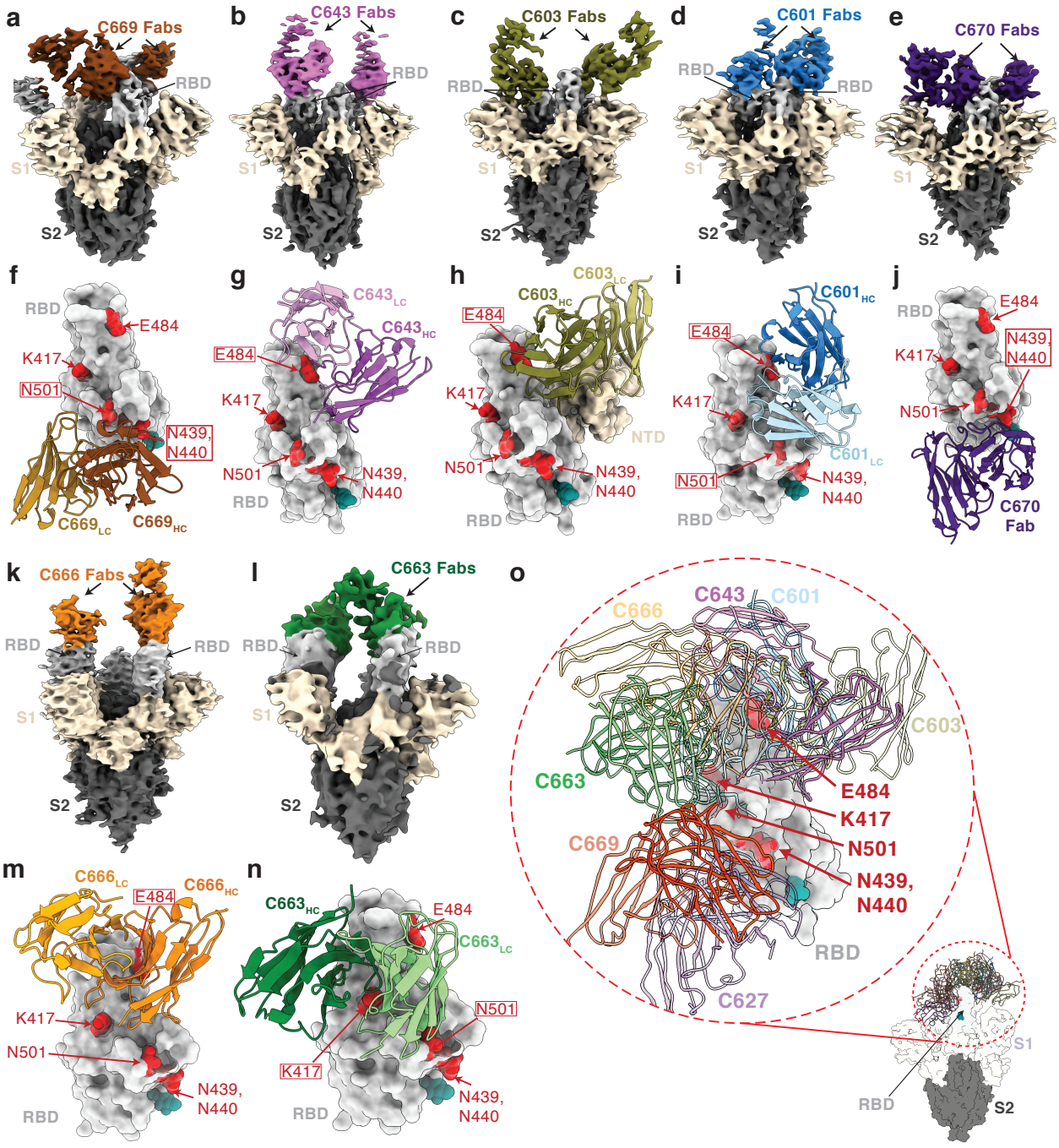

Fig. 4. Cryo-EM reconstructions of Fab-S complexes. Cryo-EM densities for Fab-S complexes (**a-e**; **k-l**) and close-up views of antibody footprints on RBDs (**f-j**; **m-n**) are shown for neutralizing mAbs. As expected due to Fab inter-domain flexibility, cryo-EM densities (**a-e**; **k-l**) were weak for the Fab C_H-C_L domains. Models of antibody footprints on RBDs (**f-j**; **m-n**) are

298 presented as Fab V_H-V_L domains (cartoon) complexed with the RBD (surface). To generate
299 models, coordinates of stabilized S trimer (PDB 6XKL) and representative Fab fragments (PDB
300 6XCA or 7K8P) with CDR3 loops removed were fit by rigid body docking into the cryo-EM
301 density maps. **a,f,** C669; **b,g,** C643; **c,h,** C603; **d,i,** C601; **e,j,** C670; **k,m,** C666; and **l,n,** C663.
302 RBD residues K417, N439, N440, E484, and N501 are highlighted as red surfaces. The N343
303 glycan is shown as a teal sphere. **o,** Composite model illustrating targeted epitopes of RBD-
304 specific neutralizing mAbs (shown as V_H-V_L domains in colors from panels **a-l**) elicited from
305 mRNA vaccines.
306

Methods

Data reporting

No statistical methods were used to predetermine sample size. The experiments were not randomized and the investigators were not blinded to allocation during experiments and outcome assessment.

Study participants.

To isolate and characterize anti-SARS-CoV-2 RBD antibodies from vaccinees, a cohort of 20 individuals that participated in either the Moderna or Pfizer-BioNTech phase 3 vaccine clinical trials and did not report prior history of SARS-CoV-2 infection was recruited at the NIH Blood Center and the Rockefeller University Hospital for blood donation. Eligible participants included adults, at least 18 years of age with no known heart, lung, kidney disease or bleeding disorders, no history of HIV-1 or malaria infection. All participants were asymptomatic at the time of the study visit and had received a complete 2 dose regimen of either mRNA vaccine. Informed consent was obtained from all participants and the study was conducted in accordance with Good Clinical Practice. The study visits and blood draws were reviewed and approved under the National Institutes of Health's Federalwide Assurance (FWA00005897), in accordance with Federal regulations 45 CFR 46 and 21 CFR 5 by the NIH Intramural Research Program IRB committee (IRB# 99CC0168, Collection and Distribution of Blood Components from Healthy Donors for In Vitro Research Use) and by the Institutional Review Board of the Rockefeller University (IRB# DRO-1006, Peripheral Blood of Coronavirus Survivors to Identify Virus-Neutralizing Antibodies). For detailed participant characteristics see Extended Data Table SI 1.

Blood samples processing and storage.

Samples collected at NIH were drawn from participants at the study visit and processed within 24 hours. Briefly, whole blood samples were subjected to Ficoll gradient centrifugation after 1:1 dilution in PBS. Plasma and PBMC samples were obtained through phase separation of plasma layer and Buffy coat phase, respectively. PBMCs were further prepared through centrifugation, red blood cells lysis and washing steps, and stored in CellBanker cell freezing media (Amsbio). All samples were aliquoted and stored at - 80 °C and shipped on dry ice. Prior to experiments, aliquots of plasma samples were heat-inactivated (56°C for 1 hour) and then stored at 4°C. Peripheral Blood Mononuclear Cells (PBMCs) obtained from samples collected at Rockefeller University were purified as previously reported[6,7] by gradient centrifugation and stored in liquid nitrogen in the presence of FCS and DMSO. Heparinized plasma samples were aliquoted and stored at -20°C or less. Prior to experiments, aliquots of plasma samples were heat-inactivated (56°C for 1 hour) and then stored at 4°C.

ELISAs

ELISAs[41,42] to evaluate antibodies binding to SARS-CoV-2 S (BioHub), RBD and additional mutated RBDs were performed by coating of high-binding 96-half-well plates (Corning 3690) with 50 µl per well of a 1µg/ml protein solution in PBS overnight at 4 °C. Plates were washed 6 times with washing buffer (1× PBS with 0.05% Tween-20 (Sigma-Aldrich)) and incubated with 170 µl per well blocking buffer (1× PBS with 2% BSA and 0.05% Tween-20 (Sigma)) for 1 h at room temperature. Immediately after blocking, monoclonal antibodies or plasma samples were added in PBS and incubated for 1 h at room temperature. Plasma samples were assayed at a

1:66.6 (RU samples) or a 1:33.3 (NIH samples) starting dilution and 7 additional threefold serial dilutions. Monoclonal antibodies were tested at 10 µg/ml starting concentration and 10 additional fourfold serial dilutions. Plates were washed 6 times with washing buffer and then incubated with anti-human IgG, IgM or IgA secondary antibody conjugated to horseradish peroxidase (HRP) (Jackson Immuno Research 109-036-088 109-035-129 and Sigma A0295) in blocking buffer at a 1:5,000 dilution (IgM and IgG) or 1:3,000 dilution (IgA). Plates were developed by addition of the HRP substrate, TMB (ThermoFisher) for 10 min (plasma samples) or 4 minutes (monoclonal antibodies), then the developing reaction was stopped by adding 50 µl 1 M H_2SO_4 and absorbance was measured at 450 nm with an ELISA microplate reader (FluoStar Omega, BMG Labtech) with Omega and Omega MARS software for analysis. For plasma samples, a positive control (plasma from participant COV72[6,7], diluted 66.6-fold and with seven additional threefold serial dilutions in PBS) was added to every assay plate for validation. The average of its signal was used for normalization of all of the other values on the same plate with Excel software before calculating the area under the curve using Prism V8.4 (GraphPad). For monoclonal antibodies, the EC50 was determined using four-parameter nonlinear regression (GraphPad Prism V8.4).

Expression of RBD proteins

Mammalian expression vectors encoding the RBDs of SARS-CoV-2 (GenBank MN985325.1; S protein residues 319-539) and eight additional mutant RBD proteins (E484K, Q493R, R346S, N493K, N440K, V367F, A475V, S477N and V483A) with an N-terminal human IL-2 or Mu phosphatase signal peptide were previously described[21].

376 **Cells and viruses**

377 293T/ACE2.cl22 and HT1080/ACE2.cl14 cells[8] were cultured in Dulbecco's Modified Eagle
378 Medium (DMEM) supplemented with 10% fetal bovine serum (FBS) at 37°C and 5% CO_2. Cells
379 were periodically tested for contamination with mycoplasma or retroviruses.
380 rVSV/SARS-CoV-2/GFP chimeric virus stocks were generated by infecting 293T/ACE2.cl22
381 cells. Supernatant was harvested 1 day post infection (dpi), cleared of cellular debris, and stored
382 at -80°C. A plaque purified variant designated rVSV/SARS-CoV-2/GFP_{2E1} that encodes
383 D215G/R683G substitutions was used in these studies[8].
384
385 **Selection and analysis of antibody escape mutations**
386 For the selection of monoclonal antibody-resistant spike variants, a rVSV/SARS-CoV-2/GFP_{2E1}
387 (for details see[8]) population containing 10^6 infectious units was incubated with of monoclonal
388 antibodies (10 μg/ml passage 10-40 μg/ml for 1 hr at 37 °C. Then, the virus-antibody mixtures
389 were incubated with 5× 10^5 293T/ACE2cl.22 cells in 6-well plates. At 1 day post infection media
390 was replaced with fresh media containing the equivalent concentrations of antibodies.
391 Supernatant was harvested 2 days after infection and 150 μl of the cleared supernatant was used
392 to infect cells for passage 2, while 150 μl was subjected to RNA extraction and sequencing.
393 For identification of putative antibody resistance mutations, RNA was extracted using
394 NucleoSpin 96 Virus Core Kit (Macherey-Nagel). The RNA was reversed transcribed using the
395 SuperScript VILO cDNA Synthesis Kit (Thermo Fisher Scientific). KOD Xtreme Hot Start DNA
396 Polymerase (Millipore Sigma) was used for amplification of cDNA using primers flanking the S-
397 encoding sequence. The PCR products were purified and sequenced as previously described[6,10].
398 Breifly, tagmentation reactions were performed using 1ul diluted cDNA, 0.25 μl Nextera TDE1

Tagment DNA enzyme (catalog no. 15027865), and 1.25 μl TD Tagment DNA buffer (catalog no. 15027866; Illumina). Next, the DNA was ligated to unique i5/i7 barcoded primer combinations using the Illumina Nextera XT Index Kit v2 and KAPA HiFi HotStart ReadyMix (2X; KAPA Biosystems) and purified using AmPure Beads XP (Agencourt), after which the samples were pooled into one library and subjected to paired-end sequencing using Illumina MiSeq Nano 300 V2 cycle kits (Illumina) at a concentration of 12pM.

For analysis of the sequencing data, the raw paired-end reads were pre-processed to remove trim adapter sequences and to remove low-quality reads (Phred quality score < 20) using BBDuk. Reads were mapped to the rVSV/SARS-CoV-2/GFP sequence using Geneious Prime (Version 2020.1.2). Mutations were annotated using Geneious Prime, with a P-value cutoff of 10^{-6}.

SARS-CoV-2 pseudotyped reporter virus

A panel of plasmids expressing RBD-mutant SAR-CoV-2 spike proteins in the context of pSARS-CoV-2-S $_{\Delta 19}$ have been described previously[10]. Additional substitutions were introduced using either PCR primer-mediated mutagenesis or with synthetic gene fragments (IDT) followed by Gibson assembly. The mutants E484K and KEN (K417N+E484K+N501Y) were constructed in the context of a pSARS-CoV-2-S $_{\Delta 19}$ variant with a mutation in the furin cleavage site (R683G). The NT50s and IC50 of these pseudotypes were compared to a wildtype SARS-CoV-2 (NC_045512) spike sequence carrying R683G in the subsequent analyses, as appropriate.

Generation of SARS-CoV-2 pseudotyped HIV-1 particles was performed as previously described[7]. Briefly, 293T cells were transfected with pNL4-3ΔEnv-nanoluc and pSARS-CoV-2-$S_{\Delta 19}$ and pseudotyped virus stocks were harvested 48 hours after transfection, filtered and stored at -80°C.

422

423 **SARS-CoV-2 pseudotype neutralization assays**

424 Plasma or monoclonal antibodies from vaccine recipients were four-fold or five-fold serially
425 diluted and then incubated with SARS-CoV-2 pseudotyped HIV-1 reporter virus for 1 h at 37 °C.
426 The antibody and pseudeotype virus mixture was added to $293T_{Ace2}$ cells[7] (for comparisons of
427 plasma from COVID-19-convalescents and vaccine recipients) or HT1080ACE2.cl14 cells[8] (for
428 analysis of spike mutants with vaccine recipient plasma or monoclonal antibodies). After 48 h
429 cells were washed with PBS and lysed with Luciferase Cell Culture Lysis 5× reagent (Promega)
430 and Nanoluc Luciferase activity in lysates was measured using the Nano-Glo Luciferase Assay
431 System (Promega) with the Glomax Navigator (Promega). The relative luminescence units were
432 normalized to those derived from cells infected with SARS-CoV-2 pseudotyped virus in the
433 absence of plasma or monoclonal antibodies. The half-maximal neutralization titers for plasma
434 (NT_{50}) or half-maximal and 90% inhibitory concentrations for monoclonal antibodies (IC_{50} and
435 IC_{90}, respectively) were determined using four-parameter nonlinear regression (least squares
436 regression method without weighting; constraints: top=1, bottom=0) (GraphPad Prism).

437

438 **Biotinylation of viral protein for use in flow cytometry**

439 Purified and Avi-tagged SARS-CoV-2 RBD was biotinylated using the Biotin-Protein Ligase-
440 BIRA kit according to manufacturer's instructions (Avidity) as described before[7]. Ovalbumin
441 (Sigma, A5503-1G) was biotinylated using the EZ-Link Sulfo-NHS-LC-Biotinylation kit
442 according to the manufacturer's instructions (Thermo Scientific). Biotinylated ovalbumin was
443 conjugated to streptavidin-BV711 (BD biosciences, 563262) and RBD to streptavidin-PE (BD
444 Biosciences, 554061) and streptavidin-AF647 (Biolegend, 405237)[7].

445

446 **Flow cytometry and single cell sorting**

447 Single-cell sorting by flow cytometry was performed as described previously[7]. Briefly,
448 peripheral blood mononuclear cells were enriched for B cells by negative selection using a pan-
449 B-cell isolation kit according to the manufacturer's instructions (Miltenyi Biotec, 130-101-638).
450 The enriched B cells were incubated in FACS buffer (1× PBS, 2% FCS, 1 mM EDTA) with the
451 following anti-human antibodies (all at 1:200 dilution): anti-CD20-PECy7 (BD Biosciences,
452 335793), anti-CD3-APC-eFluro 780 (Invitrogen, 47-0037-41), anti-CD8-APC-eFluor 780
453 (Invitrogen, 47-0086-42), anti-CD16-APC-eFluor 780 (Invitrogen, 47-0168-41), anti-CD14-
454 APC-eFluor 780 (Invitrogen, 47-0149-42), as well as Zombie NIR (BioLegend, 423105) and
455 fluorophore-labelled RBD and ovalbumin (Ova) for 30 min on ice. Single
456 CD3−CD8−CD14−CD16−CD20+Ova−RBD-PE+RBD-AF647+ B cells were sorted into
457 individual wells of 96-well plates containing 4 µl of lysis buffer (0.5× PBS, 10 mM DTT, 3,000
458 units/ml RNasin Ribonuclease Inhibitors (Promega, N2615) per well using a FACS Aria III and
459 FACSDiva software (Becton Dickinson) for acquisition and FlowJo for analysis. The sorted cells
460 were frozen on dry ice, and then stored at −80 °C or immediately used for subsequent RNA
461 reverse transcription.

462

463 **Antibody sequencing, cloning and expression**

464 Antibodies were identified and sequenced as described previously[7]. In brief, RNA from single
465 cells was reverse-transcribed (SuperScript III Reverse Transcriptase, Invitrogen, 18080-044) and
466 the cDNA stored at −20 °C or used for subsequent amplification of the variable IGH, IGL and
467 IGK genes by nested PCR and Sanger sequencing. Sequence analysis was performed using

MacVector. Amplicons from the first PCR reaction were used as templates for sequence- and ligation-independent cloning into antibody expression vectors. Recombinant monoclonal antibodies and Fabs were produced and purified as previously described[7].

Cryo-EM sample preparation

Expression and purification of SARS-CoV-2 6P stabilized S trimers[29] was conducted as previously described[43]. Purified Fab and S 6P trimer were incubated at a 1.1:1 molar ratio per protomer on ice for 30 minutes prior to deposition on a freshly glow-discharged 300 mesh, 1.2/1.3 Quantifoil copper grid. Immediately before 3 µl of complex was applied to the grid, fluorinated octyl-malotiside was added to the Fab-S complex to a final detergent concentration of 0.02% w/v, resulting in a final complex concentration of 3 mg/ml. Samples were vitrified in 100% liquid ethane using a Mark IV Vitrobot after blotting for 3 s with Whatman No. 1 filter paper at 22˚C and 100% humidity.

Cryo-EM data collection and processing

Data collection and processing followed a similar workflow to what has been previously described in detail[20]. Briefly, micrographs were collected on a Talos Arctica transmission electron microscope (Thermo Fisher) operating at 200 kV for all Fab-S complexes. Data were collected using SerialEM automated data collection software[44] and movies were recorded with a K3 camera (Gatan). For all datasets, cryo-EM movies were patch motion corrected for beam-induced motion including dose-weighting within cryoSPARC v2.15[45] after binning super resolution movies. The non-dose-weighted images were used to estimate CTF parameters using cryoSPARC implementation of the Patch CTF job. Particles were picked using Blob picker and

extracted 4x binned and 2D classified. Class averages corresponding to distinct views with secondary structure features were chosen and ab initio models were generated. 3D classes that showed features of a Fab-S complex were re-extracted, unbinned (0.869 Å/pixel) and homogenously refined with C1 symmetry. Overall resolutions were reported based on gold standard FSC calculations.

Cryo-EM Structure Modeling and Refinement

Coordinates for initial complexes were generated by docking individual chains from reference structures into cryo-EM density using UCSF Chimera[46] (S trimer: PDB 6KXL, Fab: PDB 6XCA or 7K8P after trimming CDR3 loops and converting to a polyalanine model). Models were then refined into cryo-EM maps by rigid body and real space refinement in Phenix[47] If the resolution allowed, partial CDR3 loops were built manually in Coot[48] and then refined using real-space refinement in Phenix.

Computational analyses of antibody sequences

Antibody sequences were trimmed based on quality and annotated using Igblastn v.1.14. with IMGT domain delineation system. Annotation was performed systematically using Change-O toolkit v.0.4.540 [49]. Heavy and light chains derived from the same cell were paired, and clonotypes were assigned based on their V and J genes using in-house R and Perl scripts (Extended data Fig. 2). All scripts and the data used to process antibody sequences are publicly available on GitHub (https://github.com/stratust/igpipeline).

513 The frequency distributions of human V genes in anti-SARS-CoV-2 antibodies from this study
514 was compared to 131,284,220 IgH and IgL sequences generated by [50] and downloaded from
515 cAb-Rep [51], a database of human shared BCR clonotypes available at https://cab-
516 rep.c2b2.columbia.edu/. Based on the 97 distinct V genes that make up the 4186 analyzed
517 sequences from Ig repertoire of the 14 participants present in this study, we selected the IgH and
518 IgL sequences from the database that are partially coded by the same V genes and counted them
519 according to the constant region. The frequencies shown in (Fig 2e and Extended Data Fig 3a**)**
520 are relative to the source and isotype analyzed. We used the two-sided binomial test to check
521 whether the number of sequences belonging to a specific IgHV or IgLV gene in the repertoire is
522 different according to the frequency of the same IgV gene in the database. Adjusted p-values
523 were calculated using the false discovery rate (FDR) correction. Significant differences are
524 denoted with stars.
525
526 Nucleotide somatic hypermutation and CDR3 length were determined using in-house R and Perl
527 scripts. For somatic hypermutations, IGHV and IGLV nucleotide sequences were aligned against
528 their closest germlines using Igblastn and the number of differences were considered nucleotide
529 mutations. The average mutations for V genes were calculated by dividing the sum of all
530 nucleotide mutations across all participants by the number of sequences used for the analysis. To
531 calculate the GRAVY scores of hydrophobicity[52] we used Guy H.R. Hydrophobicity scale based
532 on free energy of transfer (kcal/mole)[53] implemented by the R package Peptides (the
533 Comprehensive R Archive Network repository; https://journal.r-project.org/archive/2015/RJ-
534 2015-001/RJ-2015-001.pdf). We used 1409 heavy chain CDR3 amino acid sequences from this
535 study and 22,654,256 IGH CDR3 sequences from the public database of memory B cell receptor

sequences[54]. The two-tailed Wilcoxon nonparametric test was used to test whether there is a difference in hydrophobicity distribution.

Data availability statement: Data are provided in SI Tables 1-8. The raw sequencing data and computer scripts associated with Fig. 2 have been deposited at Github (https://github.com/stratust/igpipeline). This study also uses data from "A Public Database of Memory and Naive B-Cell Receptor Sequences" [54], PDB (6VYB and 6NB6) and from "High frequency of shared clonotypes in human B cell receptor repertoires" [50]. Cryo-EM maps associated with data reported in this manuscript will be deposited in the Electron Microscopy Data Bank (EMDB: https://www.ebi.ac.uk/pdbe/emdb/).

Data presentation

Figures arranged in Adobe Illustrator 2020.

Competing interests: The Rockefeller University has filed a provisional patent application in connection with this work on which Z.W. and M.C.N. are inventors (US patent 63/021,387).

Code availability statement: Computer code to process the antibody sequences is available at GitHub (https://github.com/stratust/igpipeline).

Acknowledgements: We thank all study participants who devoted time to our research; Drs. Barry Coller and Sarah Schlesinger, the Rockefeller University Hospital Clinical Research Support Office and nursing staff; Charles M. Rice and all members of the M.C.N. laboratory for

559 helpful discussions and Maša Jankovic for laboratory support; and Dr. Jost Vielmetter and the
560 Protein Expression Center in the Beckman Institute at Caltech for expression assistance. Electron
561 microscopy was performed in the Caltech Beckman Institute Resource Center for Transmission
562 Electron Microscopy and we thank Drs. Songye Chen and Andrey Malyutin for technical
563 assistance. This work was supported by NIH grant P01-AI138398-S1 (M.C.N. and P.J.B.) and
564 2U19AI111825 (M.C.N.); the Caltech Merkin Institute for Translational Research and P50
565 AI150464-13 (P.J.B.), a George Mason University Fast Grant (P.J.B.); R37-AI64003 to P.D.B.;
566 R01AI78788 to T.H.; We thank Dr. Jost Vielmetter and the Protein Expression Center in the
567 Beckman Institute at Caltech for expression assistance C.O.B. is supported by the HHMI Hanna
568 Gray and Burroughs Wellcome PDEP fellowships. C.G. was supported by the Robert S. Wennett
569 Post-Doctoral Fellowship, in part by the National Center for Advancing Translational Sciences
570 (National Institutes of Health Clinical and Translational Science Award program, grant UL1
571 TR001866), and by the Shapiro-Silverberg Fund for the Advancement of Translational Research.
572 P.D.B. and M.C.N. are Howard Hughes Medical Institute Investigators.
573

574 **Author Contributions:**

575 P.D.B., P.J.B., R.C., T.H., M.C.N, Z.W., F.S., Y.W. F.M. C.O.B, S.F., D.S.B., M.Cipolla.
576 conceived, designed and analyzed the experiments. M.Caskey, C.G., J.A. L, K.W. D.S.B.
577 designed clinical protocols Z.W., F.S., Y.W. F.M. C.O.B, S.F., D.S.B., M.Cipolla, J.D.S. A.G.
578 Z.Y., M.E.A., K.E.H. carried out experiments. C.G., M.Caskey, K.W. D., R.A.C., A.H., K.G.M.
579 recruited participants and executed clinical protocols. I.S., R.P, J.D., J.X. and C.U.O. processed
580 clinical samples. T.Y.O. and V.R. performed bioinformatic analysis. R.C. P.D.B., P.J.B., T.H.,
581 and M.C.N. wrote the manuscript with input from all co-authors.

Extended Data Figures

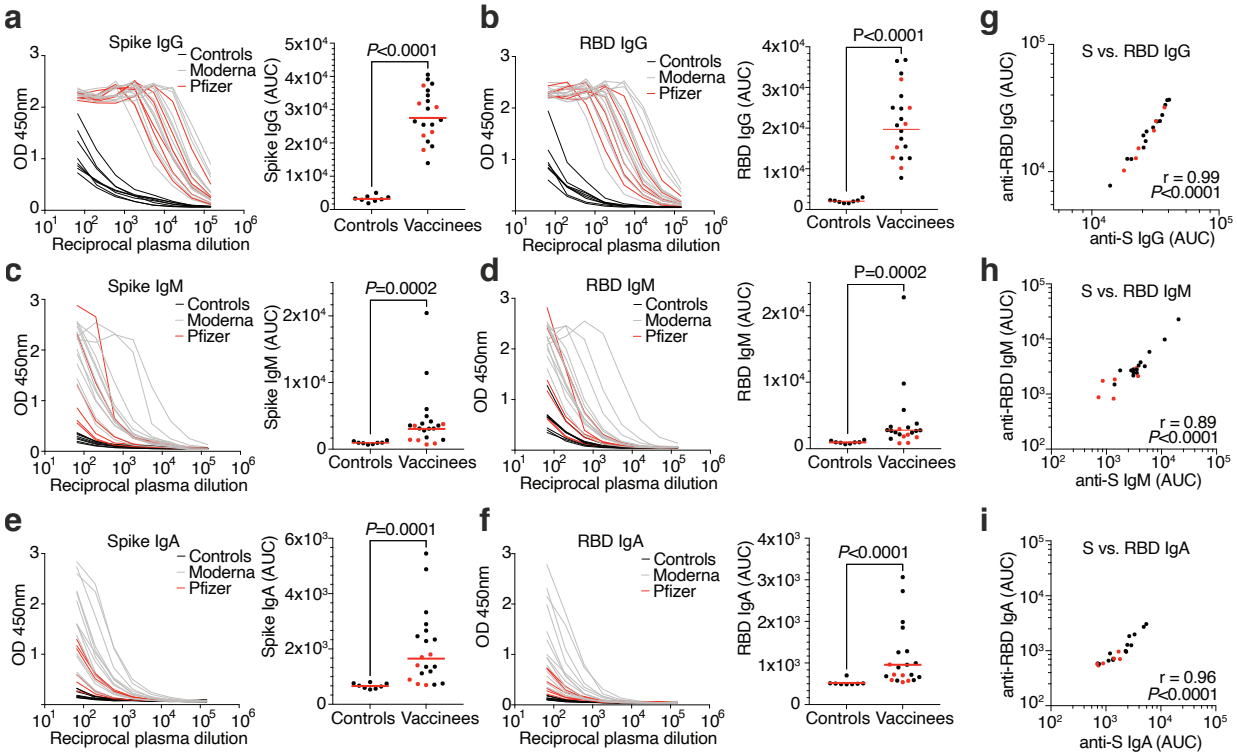

Extended Data Fig. 1. Plasma antibodies against SARS-CoV-2. **a**–**f**, Results of ELISAs measuring plasma reactivity to S (**a**,**c**,**e**) and RBD protein (**b**,**d**,**f**) of 20 vaccinees (grey curves) and 8 controls (black curves). **a**, Anti-S IgG. **b**, Anti-RBD IgG. **c**, Anti-S IgM. **d**, Anti-RBD IgM. **e**, Anti-S IgA. **f**, Anti-RBD IgA. Left, optical density at 450 nm (OD 450 nm) for the indicated reciprocal plasma dilutions. Right, normalized area under the curve (AUC) values for the 8 controls and 20 vaccinees. Horizontal bars indicate geometric mean. Statistical significance was determined using the two-tailed Mann–Whitney U-test. Average of two or more experiments. **g-i,** Correlations of plasma antibodies measurements. **g,** Normalized AUC for IgG anti-S plotted against normalized AUC for IgG anti-RBD. **h,** Normalized AUC for IgM anti-S plotted against normalized AUC for IgM anti-RBD. **i,** Normalized AUC for IgA anti-S plotted against normalized AUC for IgA anti-RBD. The *r* and *p* values in **g-i** were determined with the

595 two-tailed Spearman's correlation test. Moderna vaccinees are in black and Pfizer-BioNTech in

596 red.

597

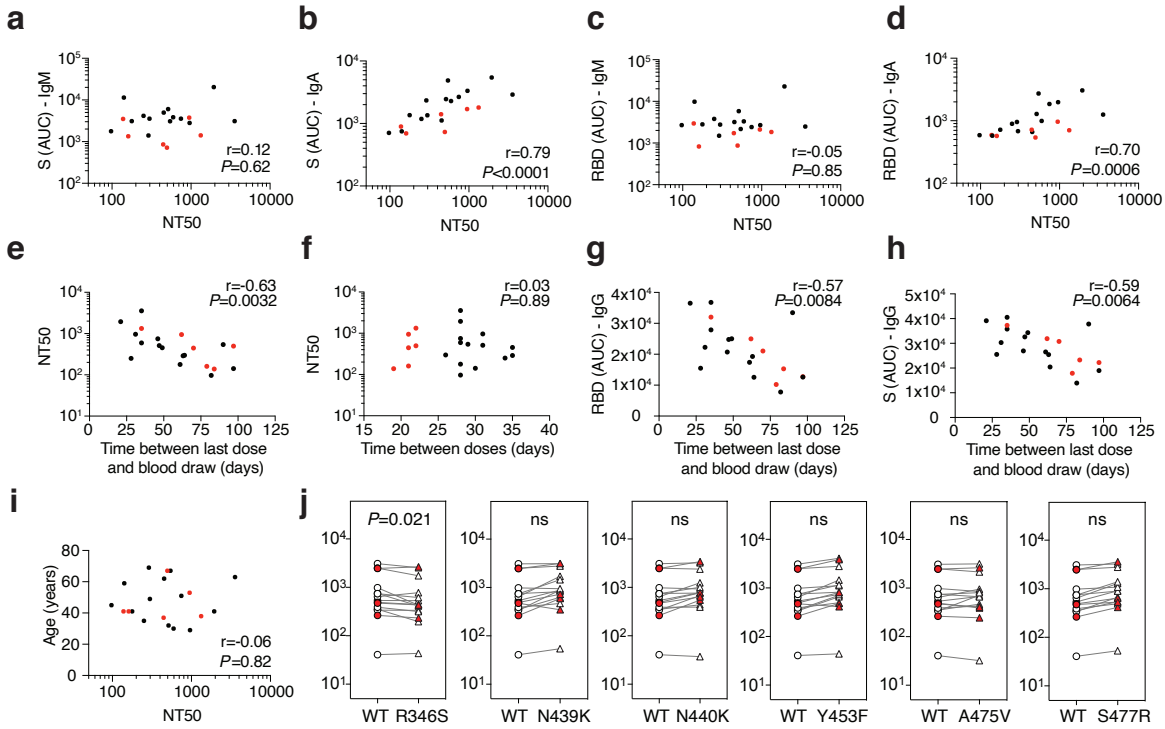

598

599 **Extended Data Fig. 2: Plasma neutralizing activity. a**, Anti-S IgM AUC (Y axis) plotted

600 against NT_{50} (X axis) r=0.12, p<0.6179. **b,** Anti-S IgA AUC (Y axis) plotted against NT_{50} (X

601 axis) r=0.79, p<0.0001. **c**, Anti-RBD IgM AUC (Y axis) plotted against NT50 (X axis) r=-0.05

602 p=0.8502. **d**, Anti-RBD IgA AUC (Y axis) plotted against NT50 (X axis) r=0.70 p=0.0006 **e**,

603 NT_{50} (Y axis) plotted against time between last dose and blood draw (X axis) r=-0.63 p=0.0032.

604 **f**, NT_{50} (Y axis) plotted against time between doses (X axis) r=0.03 p=0.8906. **g**, Anti-RBD IgG

605 AUC (Y axis) plotted against time between last dose and blood draw (X axis) r=-0.57 p=0.0084.

606 **h**, Anti-S IgG AUC (Y axis) plotted against time between last dose and blood draw (X axis) r=-

607 0.59 p=0.0064. **i**, Age (Y axis) plotted against NT_{50} (X axis) r=-0.06 p=0.8150. The r and p

608 values were determined by two-tailed Spearman's. Moderna vaccinees in black and Pfizer-

609 BioNTech in red. **j**, NT50 values for vaccinee plasma (n=15) neutralization of pseudotyped

610 viruses with WT and the indicated RBD-mutant SARS-CoV-2 S proteins; p-values determined

611 using one tailed t-test.

612

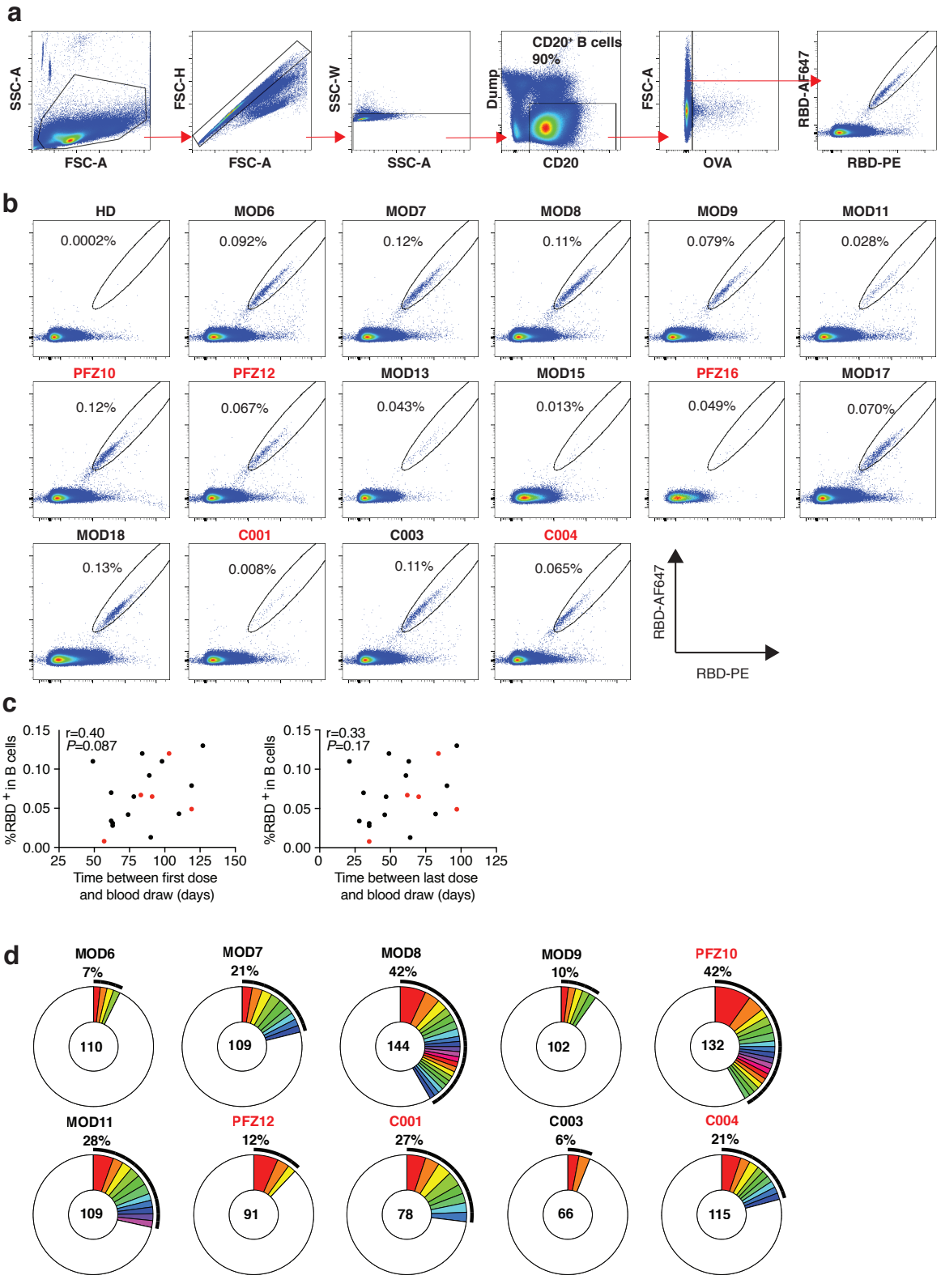

613

614 **Extended Data Fig. 3: Flow cytometry. a,** Gating strategy used for cell sorting. Gating was on
615 singlets that were CD20+ and CD3-CD8-CD16-OVA-. Sorted cells were RBD-PE+ and RBD-
616 AF647+. **b,** Flow cytometry showing the percentage of RBD-double positive memory B cells
617 from a pre-COVID-19 control (HD) and 15 vaccinees, who received the Moderna vaccine are
618 shown in black and Pfizer-BioNTech vaccine recipients are in red. **c**, the percentage of RBD-
619 binding memory B cells in vaccinees (Y axis) plotted against time between first dose and blood
620 draw (X axis) r=0.4028 p=0.0873 (left panel), and between last dose and blood draw (X axis)
621 r=0.3319 p=0.1651 (right panel). Moderna vaccinees in black and Pfizer-BioNTech in red. The r
622 and p values for correlations were determined by two-tailed Spearman's. **d,** Pie charts show the
623 distribution of antibody sequences from 10 individuals in **b.** The number in the inner circle
624 indicates the number of sequences analyzed. Pie slice size is proportional to the number of
625 clonally related sequences. The black outline indicates the frequency of clonally expanded
626 sequences. The r and p values for correlations in **c** were determined by the two-tailed Spearman
627 correlation test.
628

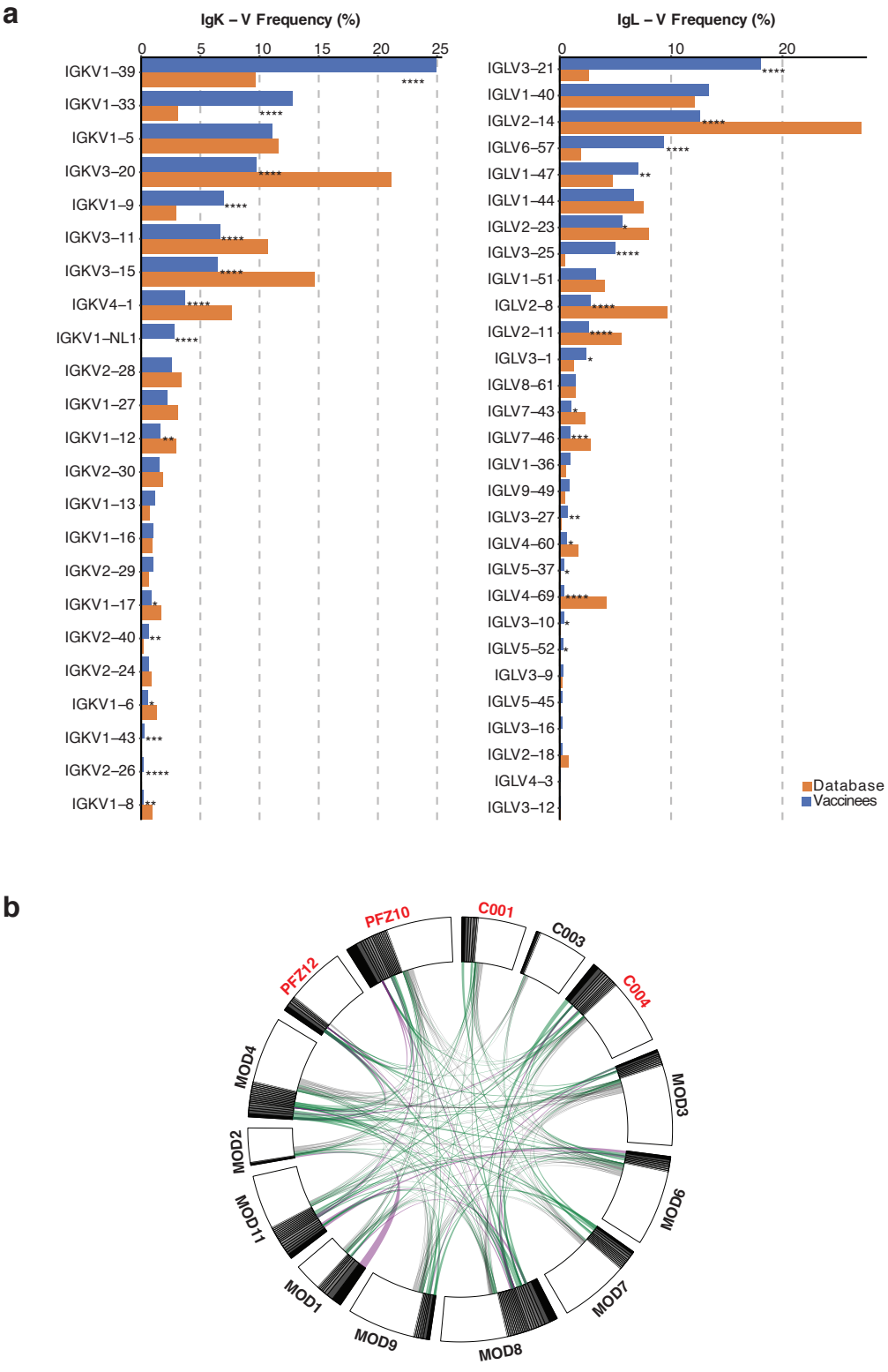

Extended Data Fig. 4: Frequency distributions of human VL genes.

631 Graph shows relative abundance of human IGVK (left) and IgVL (right) genes of Sequence Read
632 Archive accession SRP010970 (orange)[55], and vaccinees (blue). Two-sided binomial tests with
633 unequal variance were used to compare the frequency distributions., significant differences are
634 denoted with stars. (* $p < 0.05$, ** $p < 0.01$, *** $p < 0.001$, **** = $p < 0.0001$). **b.** Sequences
635 from 14 individuals (Extended Data Table 2) with clonal relationships depicted as in **c.**
636 Interconnecting lines indicate the relationship between antibodies that share V and J gene
637 segment sequences at both IGH and IGL. Purple, green and grey lines connect related clones,
638 clones and singles, and singles to each other, respectively.
639

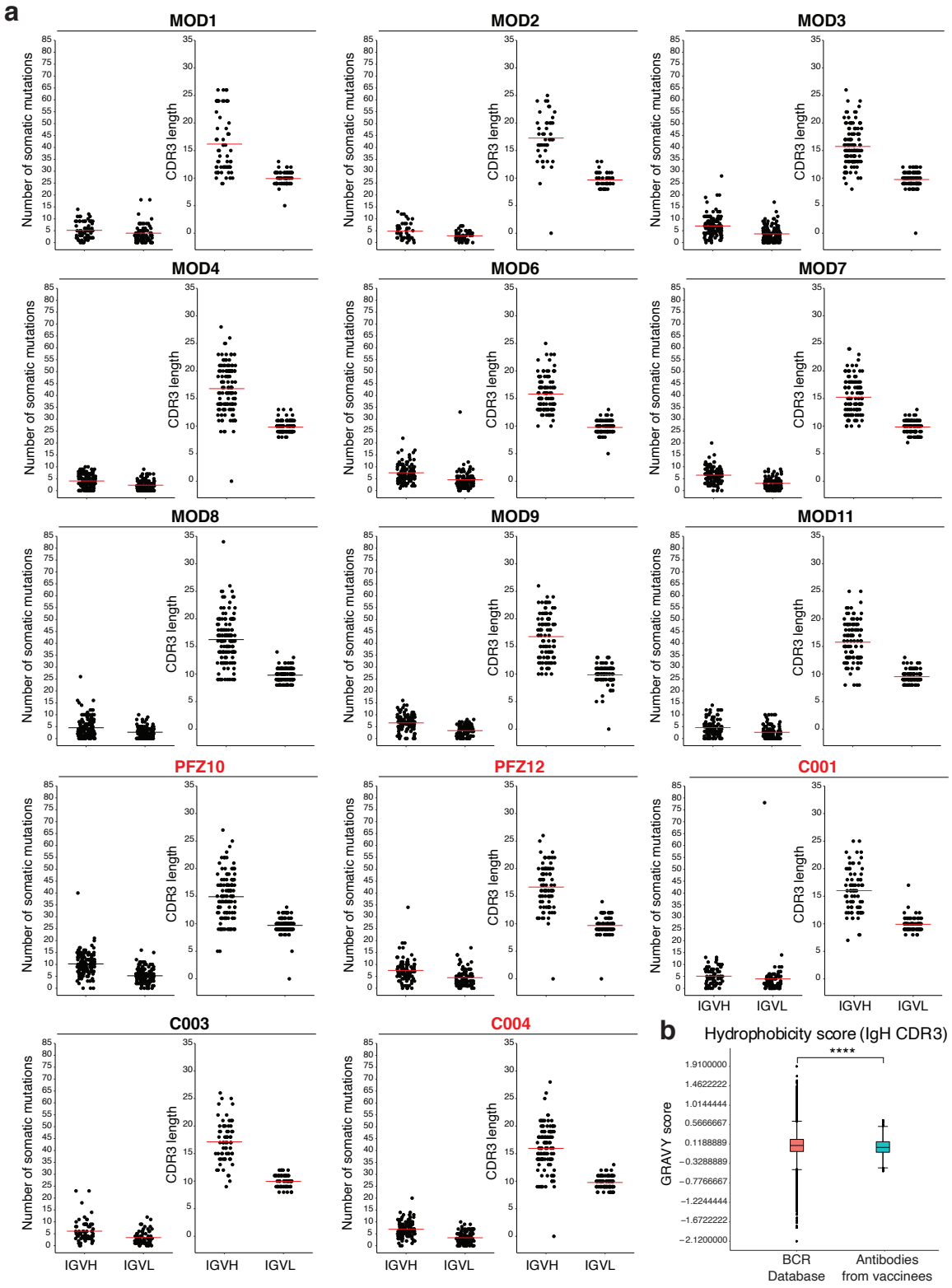

640

Extended Data Fig. 5: Antibody somatic hypermutation, and CDR3 length. a, Number of somatic nucleotide mutations in both the IGVH and IGVL in 14 participants (left). Individuals who received the Moderna vaccine are shown in black and Pfizer-BioNTech vaccine recipients in red. For each individual, the number of the amino acid length of the CDR3s at the IGVH and IGVL is shown (right). The horizontal bars indicate the mean. The number of antibody sequences (IGVH and IGVL) evaluated for each participant are n=68 (MOD1), n=45 (MOD2), n=117 (MOD3), n=123 (MOD4), n=110 (MOD6), n=109 (MOD7), n=144 (MOD8), n=102 (MOD9), n=132 (PFZ10), n=109 (MOD11), n=91 (PFZ12), n=78 (C001), n=66 (C003), and n=115 (C004). **b,** Distribution of the hydrophobicity GRAVY scores at the IGH CDR3 compared to a public database (see Methods for statistical analysis). The box limits are at the lower and upper quartiles, the center line indicates the median, the whiskers are 1.5× interquartile range and the dots represent outliers. Statistical significance was determined using two-tailed Wilcoxon matched-pairs signed rank test (n.s.=non-significant, **** = $p < 0.0001$).

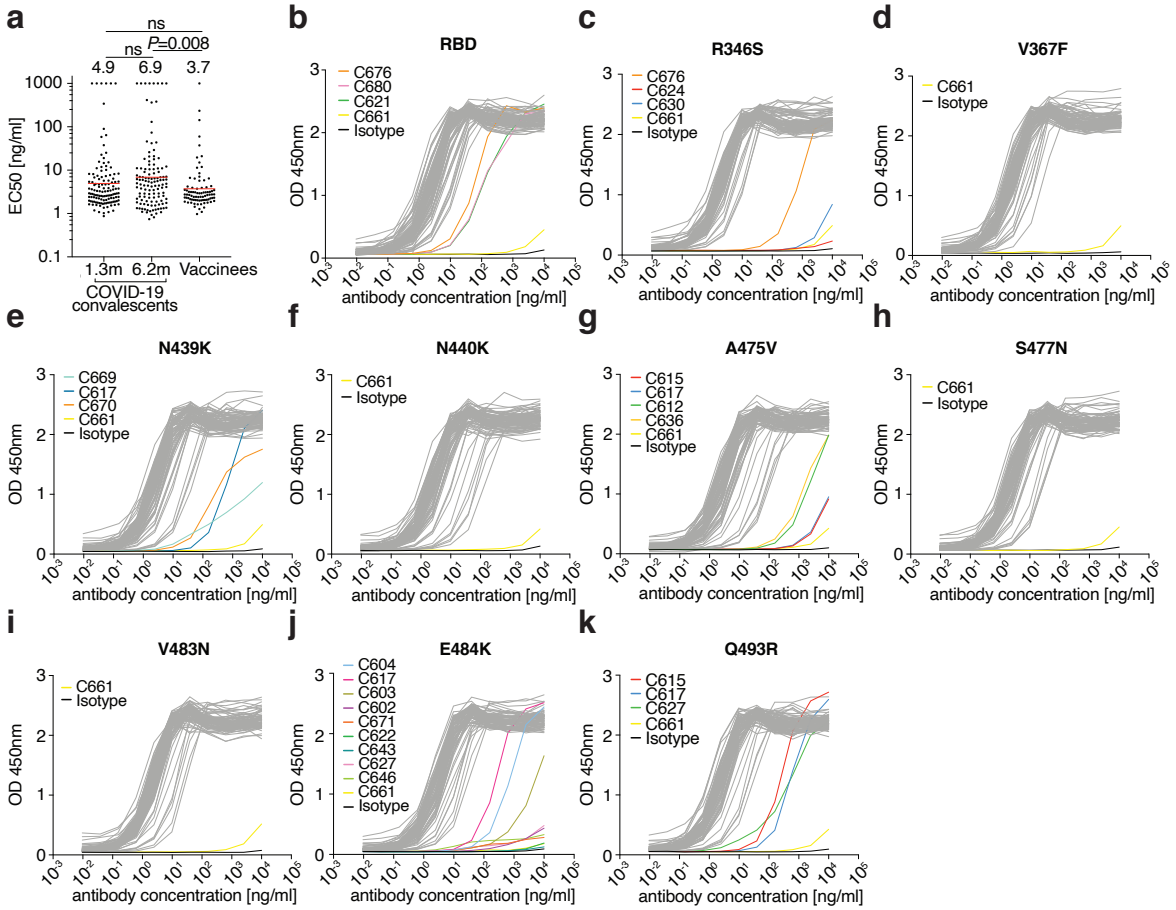

l

		wt	R346S	V367F	N439K	N440K	A475V	S477N	V483A	E484K	Q493R
Class 1	C682	2.4	2.2	2.6	3.6	3.5	35.0	3.3	2.8	3.7	4.1
	C613	2.0	1.9	1.8	3.3	2.5	126.1	2.4	2.3	2.2	4.9
	C663	1.9	1.8	1.7	2.7	2.5	12.6	2.3	2.0	2.4	2.2
	C614	1.4	1.6	1.6	2.0	1.9	2.5	1.8	1.9	1.6	1.8
	C660	2.0	2.0	2.1	2.3	2.7	2.5	2.1	2.2	2.4	2.2
Class 1/2	C653	2.1	2.1	2.1	2.5	2.6	2.2	2.1	2.3	4.0	3.1
Class 2	C627	1.6	1.6	1.8	2.0	2.0	2.1	1.9	1.8	1000	1000
	C602	2.0	1.8	1.9	2.1	2.2	2.2	2.1	3.1	1000	1.9
	C671	2.3	1.7	1.5	2.4	2.4	2.5	2.0	1.8	1000	2.5
	C643	2.1	2.2	2.3	2.0	2.2	1.7	1.8	2.5	1000	1.9
Class 2/3	C603	2.1	1.7	1.7	2.1	2.2	2.3	2.0	1.9	1000	1.9
	C628	2.7	1.9	2.0	4.3	3.2	3.1	2.4	2.4	10.0	3.2
Class 3	C669	2.3	2.1	2.2	950.6	291.8	2.1	2.1	2.2	2.4	2.2
	C670	2.9	2.1	2.3	210.7	2.8	3.0	2.6	2.4	3.3	3.3
Unclassified	C666	1.9	1.7	1.8	2.0	2.1	1.5	1.8	1.9	2.1	1.8
	C601	1.1	1.8	2.1	2.2	2.2	1.9	1.9	2.2	12.1	2.0
	C675	1.3	1.1	1.4	1.8	1.7	3.5	1.4	1.5	1.6	1.4

655

Extended Data Fig. 6: Monoclonal antibody ELISAs. a, Graph shows antibody binding to SARS-CoV-2 RBD. ELISA EC_{50} (half-maximal response) values for 84 antibodies isolated from Moderna vaccinees measured at 8 weeks after the boost and from convalescent individuals at 1.3 and 6.2 months[6,7]. Horizontal bars indicate geometric mean. Statistical significance was determined using the two-tailed Mann–Whitney U-test. Average of two or more experiments. **b-k,** Graphs show ELISA titrations for antibodies all 84 antibodies against the indicated RBD variants. n = 84 samples and isotype antibody as indicated in the figure. Low-binding antibodies are indicated in colors. Data are representative of two independent experiments. **l,** Table shows a heat map summary of EC_{50} values for binding to wild type RBD and the indicated mutants for 17 top neutralizing antibodies.

Supplementary Tables

Supplementary Table 1: Individual vaccinee characteristics

SI Table 1. Individual vaccinee characteristics

	Demographic characteristics				Vaccination details				Serological assays									
						# of doses received	Time between (days)			S protein (AUC)			RBD (AUC)			Neutralization titer (reciprocal dilution)		Flow cytometry and antibody cloning	
Participant ID	Age (years)	Sex	Race §	Ethnicity	Vaccine platform		1st & 2nd dose	1st dose & blood draw	2nd dose & blood draw	IgG	IgM	IgA	IgG	IgM	IgA	NT50	NT90	B cell phenotyping and Ig sequencing	Monoclonal antibodies expressed
MOD1	51	Male	W	Hispanic	Moderna	2	28	74	46	26940	3563	2663	20704	2420	1850	746	88	Yes/Yes	Yes
MOD2	35	Male	W	Non-Hispanic	Moderna	2	34	62	28	25504	4164	1187	15479	3784	894	250	33	Yes/Yes	Yes
MOD3	32	Male	W	Non-Hispanic	Moderna	2	31	78	47	32594	6028	2460	24797	5827	1282	513	73	Yes/Yes	Yes
MOD4	63	Female	W	Hispanic	Moderna	2	28	63	35	40526	3097	2897	36772	2483	1257	3567	587	Yes/Yes	Yes
MOD6	41	Female	W	Non-Hispanic	Moderna	2	28	89	61	26504	3109	1362	17388	2810	717	178	21	Yes/Yes	No
MOD7	62	Male	A	Non-Hispanic	Moderna	2	35	84	49	34325	4967	1120	25025	3194	662	452	80	Yes/Yes	No
MOD8	69	Female	W	Non-Hispanic	Moderna	2	35	96	63	25449	1406	2342	19284	1495	958	290	56	Yes/Yes	No
MOD9	67	Female	W	Non-Hispanic	Moderna	2	29	119	90	37818	3078	4881	33456	2172	2728	543	99	Yes/Yes	No
PFZ10	41	Male	W	Non-Hispanic	Pfizer/BioNTech	2	19	103	84	23279	3520	892	15275	2952	590	138	20	Yes/Yes	No
MOD11	30	Male	W	Non-Hispanic	Moderna	2	28	63	35	35789	3850	2287	27896	3307	994	594	111	Yes/Yes	No
PFZ12	53	Female	W	Non-Hispanic	Pfizer/BioNTech	2	21	83	62	31885	3764	1702	24996	2116	963	948	154	Yes/Yes	No
MOD13	45	Male	W	Non-Hispanic	Moderna	2	28	110	82	13938	1776	708	7767	2683	589	97	10	Yes/No	No
MOD15	49	Male	W	Non-Hispanic	Moderna	2	26	90	64	20451	3553	1354	12557	2776	680	298	46	Yes/No	No
PFZ16	67	Female	W	Non-Hispanic	Pfizer/BioNTech	2	22	119	97	22220	718	731	12741	872	539	496	60	Yes/No	No
MOD17	29	Male	AA	Non-Hispanic	Moderna	2	31	62	31	30322	2816	3325	22258	2685	1985	961	220	Yes/No	No
MOD18	59	Female	W	Non-Hispanic	Moderna	2	30	127	97	18999	11442	751	12621	9797	576	141	28	Yes/No	No
C001	38	Female	W	Non-Hispanic	Pfizer/BioNTech	2	22	57	35	37288	1418	1802	32003	1848	705	1329	268	Yes/Yes	No
C002	41	Male	W	Non-Hispanic	Pfizer/BioNTech	2	21	100	79	17898	1348	695	10205	825	572	160	36	Yes/No	No
C003	41	Male	W	Non-Hispanic	Moderna	2	28	49	21	39139	20424	5451	36509	22772	3065	1946	501	Yes/Yes	No
C004	37	Male	W	Non-Hispanic	Pfizer/BioNTech	2	21	91	70	30773	858	1409	21052	1733	720	444	115	Yes/Yes	No

§ = White (W); African American (AA); Asian (A), American Indian or Alaska Native (AI/AN); Pacific Islander (PI); Multiple (M); unknown (N/A)
All serological parameters reported here are derived from plasma samples. Reported data are the mean of two independent experiments.

Supplementary Table 2: Antibody sequences from vaccinees is provided as a separate Excel file.

Supplementary Table 3: CDR3 alignment of highly identical clonal sequences.

SI Table 3. CDR3 alignment of highly identical clonal sequences

	Heavy chain				Light chain		
	IGHV	IGHD	IGHJ	CDRH3	IGLV	IGLJ	CDRL3
MOD8	IGHV1-58*01	IGHD2-15*01	IGHJ3*02	**AAPYCSGGSCYDAFDI**	IGKV3-20*01	IGKJ1*01	**QQYGSSPWT**
	IGHV1-58*01	IGHD2-15*01	IGHJ3*02	.....	IGKV3-20*01	IGKJ1*01	.....
	IGHV1-58*01	IGHD2-15*01	IGHJ3*02	.....	IGKV3-20*01	IGKJ1*01	.....
C004	IGHV1-58*01	IGHD2-15*01	IGHJ3*02	.....N.V.H.G...	IGKV3-20*01	IGKJ1*01	...DR....
MOD3	IGHV1-58*01	IGHD2-8*01	IGHJ3*02	.....T...G.N.	IGKV3-20*01	IGKJ1*01	.....
PFZ10	IGHV4-31*03	IGHD4-23*01	IGHJ4*02	**ARDYGGNSNYFGY**	IGKV1-33*01	IGKJ4*01	**QQYNNLPLT**
	IGHV4-31*03	IGHD4-23*01	IGHJ4*02	.....A...D.	IGKV1-33*01	IGKJ4*01	...GY....
MOD11	IGHV4-31*03	IGHD4-23*01	IGHJ4*02	.....	IGKV1-33*01	IGKJ4*01	...D.....
	IGHV4-31*03	IGHD4-23*01	IGHJ4*02	...F.....D.	IGKV1-33*01	IGKJ4*01	...D.....
MOD8	IGHV4-31*03	IGHD4-23*01	IGHJ4*02	...F.....A.	IGKV1-33*01	IGKJ4*01	...D.....

Supplementary Table 4: Sequences, half maximal effective concentrations (EC50s) and inhibitory concentrations (IC50s) of the cloned monoclonal antibodies is provided as a separate Excel file.

Supplementary Table 5: Neutralization activity of mAbs against mutant SARS-CoV-2 pseudoviruses.

SI Table 5. Neutralization activity of mAbs against mutant SARS-CoV-2 pseudoviruses

	wt		R683G		R346S		K417N		N439K		N440K		Y453F		A475V		S477R		R683G/E484K		Q493R		N501Y		D614G	
	IC50 [ng/ml]	IC90 [ng/ml]	IC50 [ng/ml]	IC90 [ng/ml]	IC50 [ng/ml]	IC90 [ng/ml]	IC50 [ng/ml]	IC90 [ng/ml]	IC50 [ng/ml]	IC90 [ng/ml]	IC50 [ng/ml]	IC90 [ng/ml]	IC50 [ng/ml]	IC90 [ng/ml]	IC50 [ng/ml]	IC90 [ng/ml]	IC50 [ng/ml]	IC90 [ng/ml]	IC50 [ng/ml]	IC90 [ng/ml]	IC50 [ng/ml]	IC90 [ng/ml]	IC50 [ng/ml]	IC90 [ng/ml]	IC50 [ng/ml]	IC90 [ng/ml]
C601	2.0	9.2	1.4	6.3	1.9	11.5	1.4	6.4	1.8	8.5	2.2	10.2	1.2	7.9	1.8	11.9	1.9	8.3	112.2	630.3	2.6	13.5	4.9	13.8	2.5	8.5
C602	13.5	170.2	10.3	142.3	7.8	75.8	4.8	37.0	15.8	224.3	16.3	185.2	13.1	210.4	11.2	111.9	13.5	116.3	>1000	>1000	57.6	>1000	82.4	684.6	9.9	70.6
C603	14.3	129.9	6.7	89.5	208.7	>1000	4.9	38.8	11.8	170.2	13.2	115.1	11.7	163.0	19.1	208.3	11.3	112.5	>1000	>1000	7.1	78.5	56.1	292.9	10.8	130.7
C613	20.4	127.1	16.4	93.8	12.4	97.7	273.1	>1000	45.3	224.7	22.3	119.4	46.7	311.3	>1000	>1000	32.9	261.2	30.0	105.7	236.3	>1000	>1000	>1000	13.3	105.0
C614	5.0	20.2	3.7	16.9	4.1	26.7	>1000	>1000	3.9	20.7	5.7	23.1	4.7	34.6	31.7	215.3	4.4	20.2	9.4	26.6	6.6	41.5	16.1	37.1	4.2	17.6
C627	4.8	39.3	2.5	21.8	3.7	43.6	6.6	104.1	3.4	25.7	4.5	35.6	4.2	46.7	3.9	43.6	2.7	16.3	>1000	>1000	>1000	>1000	18.3	75.2	4.2	22.5
C628	18.8	169.9	11.6	144.3	8.6	95.3	5.2	63.4	257.3	>1000	29.8	216.2	36.5	570.6	16.1	120.1	17.9	147.2	>1000	>1000	146.8	>1000	>1000	>1000	13.6	98.4
C643	1.5	9.9	0.9	3.6	1.4	10.5	1.5	6.6	1.8	12.6	2.0	10.4	0.7	5.2	1.6	9.9	1.8	7.2	>1000	>1000	1.3	10.9	6.3	14.5	2.5	10.6
C653	9.7	45.7	7.4	42.4	6.6	47.5	>1000	>1000	7.7	36.0	9.3	43.0	18.7	109.8	20.0	126.2	10.0	41.1	>1000	>1000	168.3	875.2	34.3	100.7	8.4	39.9
C660	5.8	35.4	4.4	25.8	5.1	46.1	412.7	>1000	8.7	40.6	7.8	31.4	5.2	38.2	7.5	39.0	5.0	28.8	10.7	27.1	8.2	47.7	16.7	44.4	5.2	24.5
C663	11.5	103.7	8.5	90.6	7.6	91.7	79.6	>1000	18.9	222.4	14.4	91.7	14.4	158.5	382.1	>1000	16.5	154.1	31.7	143.3	60.2	922.1	>1000	>1000	11.5	117.8
C666	3.7	19.2	2.3	11.7	3.6	20.6	2.1	10.5	3.0	14.7	4.0	19.5	2.8	17.0	6.7	72.9	3.4	13.2	239.8	901.3	4.2	32.8	10.0	29.7	3.7	13.6
C669	15.5	183.0	17.5	164.1	9.4	169.1	12.0	96.1	>1000	>1000	>1000	>1000	20.4	154.0	13.3	172.5	13.5	146.3	24.1	258.5	13.1	177.3	141.0	469.8	16.7	84.6
C670	13.8	168.9	12.1	125.2	10.1	148.8	7.6	73.7	>1000	>1000	15.9	87.7	16.6	219.6	12.4	129.6	10.8	156.0	50.4	246.3	15.4	296.2	>1000	>1000	13.2	85.1
C671	5.4	37.8	3.1	22.7	5.9	47.1	4.5	29.2	4.8	33.1	6.9	35.3	5.6	38.8	5.9	42.3	4.7	34.5	>1000	>1000	282.8	>1000	27.7	84.4	5.1	24.3
C675	19.5	111.6	12.3	92.9	15.0	129.3	11.3	76.8	17.2	78.9	22.7	105.5	18.1	140.4	38.3	225.3	15.0	91.5	23.9	78.1	13.7	110.8	71.3	190.9	13.3	82.3
C682	45.3	196.0	29.4	191.9	25.9	199.6	>1000	>1000	23.3	132.0	43.2	215.0	12.4	85.3	>1000	>1000	62.3	367.1	110.4	478.6	214.3	>1000	383.2	>1000	28.0	232.8

681

682 **Supplementary Table 6: Cryo-EM data collection and processing statistics**

Table S6. Cryo-EM data collection and processing statistics

	C601 Fab SARS-CoV-2 S 6P	C603 Fab SARS-CoV-2 S 6P	C643 Fab SARS-CoV-2 S 6P	C663 Fab SARS-CoV-2 S 6P	C666 Fab SARS-CoV-2 S 6P	C669 Fab SARS-CoV-2 S 6P	C670 Fab SARS-CoV-2 S 6P
EMD	xxxx	xxxx	xxxx	xxxx	xxxx	xxxx	xxxx
Data collection conditions							
Microscope	Talos Arctica	Talos Artica	Talos Artica	Talos Artica	Talos Arctica	Talos Artica	Talos Artica
Camera	Gatan K3 Summit	Gatan K3 Summit	Gatan K3 Summit	Gatan K3 Summit	Gatan K3 Summit	Gatan K3 Summit	Gatan K3 Summit
Magnification	45,000x	45,000x	45,000x	45,000x	45,000x	45,000x	45,000x
Voltage (kV)	200	200	200	200	200	200	200
Recording mode	counting	counting	counting	counting	counting	counting	counting
Dose rate (e /pixel/s)	13.5	13.5	13.8	13.3	13.5	13.8	13.3
Electron dose (e /Å^2)	60	60	60	60	60	60	60
Defocus range (μm)	0.7 – 2.0	0.7 – 2.0	0.7 – 2.0	0.7 – 2.0	0.7 – 2.0	0.7 – 2.0	0.7 – 2.0
Pixel size (Å)	0.8689	0.8689	0.8689	0.8689	0.8689	0.8689	0.8689
Micrographs collected	846	1,053	1,849	1,200	2,059	1,961	1,863
Micrographs used	796	1,053	1,487	1,005	1,975	1,720	1,863
Total extracted particles	187,627	490,663	340,563	268,485	256,500	265,364	596,506
Refined particles	101,271	57,573	117,987	108,407	127,936	129,917	140,171
Particles in final refinement	37,665	57,573	54,392	48,088	42,582	54,129	140,171
Symmetry imposed	C1	C1	C1	C1	C1	C1	C1
FSC=0.143 Resolution (Å)	6.5	6.4	5.0	8.3	5.1	4.9	6.9

683

684

685

References

1 Gaebler, C. & Nussenzweig, M. C. All eyes on a hurdle race for a SARS-CoV-2 vaccine. *Nature* **586**, 501-502, doi:10.1038/d41586-020-02926-w (2020).

2 Krammer, F. SARS-CoV-2 vaccines in development. *Nature* **586**, 516-527, doi:10.1038/s41586-020-2798-3 (2020).

3 Jackson, L. A. *et al.* An mRNA Vaccine against SARS-CoV-2 - Preliminary Report. *N Engl J Med* **383**, 1920-1931, doi:10.1056/NEJMoa2022483 (2020).

4 Polack, F. P. *et al.* Safety and Efficacy of the BNT162b2 mRNA Covid-19 Vaccine. *N Engl J Med* **383**, 2603-2615, doi:10.1056/NEJMoa2034577 (2020).

5 Walsh, E. E. *et al.* Safety and Immunogenicity of Two RNA-Based Covid-19 Vaccine Candidates. *N Engl J Med* **383**, 2439-2450, doi:10.1056/NEJMoa2027906 (2020).

6 Gaebler, C. *et al.* Evolution of Antibody Immunity to SARS-CoV-2. *bioRxiv*, doi:10.1101/2020.11.03.367391 (2020).

7 Robbiani, D. F. *et al.* Convergent antibody responses to SARS-CoV-2 in convalescent individuals. *Nature* **584**, 437-442, doi:10.1038/s41586-020-2456-9 (2020).

8 Schmidt, F. *et al.* Measuring SARS-CoV-2 neutralizing antibody activity using pseudotyped and chimeric viruses. *J Exp Med* **217**, doi:10.1084/jem.20201181 (2020).

9 Widge, A. T. *et al.* Durability of Responses after SARS-CoV-2 mRNA-1273 Vaccination. *N Engl J Med* **384**, 80-82, doi:10.1056/NEJMc2032195 (2021).

10 Weisblum, Y. *et al.* Escape from neutralizing antibodies by SARS-CoV-2 spike protein variants. *Elife* **9**, doi:10.7554/eLife.61312 (2020).

11 Baum, A. *et al.* Antibody cocktail to SARS-CoV-2 spike protein prevents rapid mutational escape seen with individual antibodies. *Science* **369**, 1014-1018, doi:10.1126/science.abd0831 (2020).

12 Davies, N. G. *et al.* Estimated transmissibility and severity of novel SARS-CoV-2 Variant of Concern 202012/01 in England. *medRxiv*, 2020.2012.2024.20248822, doi:10.1101/2020.12.24.20248822 (2020).

13 Greaney, A. J. *et al.* Comprehensive mapping of mutations to the SARS-CoV-2 receptor-binding domain that affect recognition by polyclonal human serum antibodies. **588**, 682-635, doi:10.1101/2020.12.31.425021 (2021).

14 Greaney, A. J. *et al.* Complete Mapping of Mutations to the SARS-CoV-2 Spike Receptor-Binding Domain that Escape Antibody Recognition. *Cell Host Microbe* **29**, 44-57 e49, doi:10.1016/j.chom.2020.11.007 (2021).

15 Japan, N. I. o. I. D. Brief report: New Variant Strain of SARS-CoV-2 Identified in Travelers from Brazil. doi:https://www.niid.go.jp/niid/images/epi/corona/covid19-33-en-210112.pdf (2021).

16 Lauring, A. S. & Hodcroft, E. B. Genetic Variants of SARS-CoV-2-What Do They Mean? *JAMA*, doi:10.1001/jama.2020.27124 (2021).

17 Tegally, H. *et al.* Emergence and rapid spread of a new severe acute respiratory syndrome-related coronavirus 2 (SARS-CoV-2) lineage with multiple spike mutations in South Africa. *medRxiv*, 2020.2012.2021.20248640, doi:10.1101/2020.12.21.20248640 (2020).

18 Briney, B., Inderbitzin, A., Joyce, C. & Burton, D. R. Commonality despite exceptional diversity in the baseline human antibody repertoire. *Nature* **566**, 393-397, doi:10.1038/s41586-019-0879-y (2019).

19 Andreano, E. *et al.* SARS-CoV-2 escape in vitro from a highly neutralizing COVID-19 convalescent plasma. *bioRxiv* **5**, 237-236, doi:10.1101/2020.12.28.424451 (2020).
20 Barnes, C. O. *et al.* SARS-CoV-2 neutralizing antibody structures inform therapeutic strategies. *Nature* **588**, 682-687, doi:10.1038/s41586-020-2852-1 (2020).
21 Barnes, C. O. *et al.* Structures of Human Antibodies Bound to SARS-CoV-2 Spike Reveal Common Epitopes and Recurrent Features of Antibodies. *Cell* **182**, 828-842 e816, doi:10.1016/j.cell.2020.06.025 (2020).
22 Thomson, E. C. *et al.* The circulating SARS-CoV-2 spike variant N439K maintains fitness while evading antibody-mediated immunity. *bioRxiv*, 2020.2011.2004.355842, doi:10.1101/2020.11.04.355842 (2020).
23 Tortorici, M. A. *et al.* Ultrapotent human antibodies protect against SARS-CoV-2 challenge via multiple mechanisms. *Science* **370**, 950-957, doi:10.1126/science.abe3354 (2020).
24 Starr, T. N. *et al.* Prospective mapping of viral mutations that escape antibodies used to treat COVID-19. *bioRxiv*, 2020.2011.2030.405472, doi:10.1101/2020.11.30.405472 (2020).
25 Lauring, A. S. & Hodcroft, E. B. Genetic Variants of SARS-CoV-2-What Do They Mean? *JAMA*, 1-3, doi:10.1001/jama.2020.27124 (2021).
26 Singer, J., Gifford, R., Cotten, M. & Robertson, D. CoV-GLUE: A Web Application for Tracking SARS-CoV-2 Genomic Variation. *Preprints*, doi:10.20944/preprints202006.0225.v1 (2020).
27 Elbe, S. & Buckland-Merrett, G. Data, disease and diplomacy: GISAID's innovative contribution to global health. *Glob Chall* **1**, 33-46, doi:10.1002/gch2.1018 (2017).
28 Voloch, C. M. *et al.* Genomic characterization of a novel SARS-CoV-2 lineage from Rio de Janeiro, Brazil. *medRxiv* (2020).
29 Hsieh, C. L. *et al.* Structure-based design of prefusion-stabilized SARS-CoV-2 spikes. *Science* **369**, 1501-1505, doi:10.1126/science.abd0826 (2020).
30 Brouwer, P. J. M. *et al.* Potent neutralizing antibodies from COVID-19 patients define multiple targets of vulnerability. *Science* **369**, 643-650, doi:10.1126/science.abc5902 (2020).
31 Cao, Y. *et al.* Potent Neutralizing Antibodies against SARS-CoV-2 Identified by High-Throughput Single-Cell Sequencing of Convalescent Patients' B Cells. *Cell* **182**, 73-84 e16, doi:10.1016/j.cell.2020.05.025 (2020).
32 Ju, B. *et al.* Human neutralizing antibodies elicited by SARS-CoV-2 infection. *Nature* **584**, 115-119, doi:10.1038/s41586-020-2380-z (2020).
33 Liu, L. *et al.* Potent neutralizing antibodies against multiple epitopes on SARS-CoV-2 spike. *Nature* **584**, 450-456, doi:10.1038/s41586-020-2571-7 (2020).
34 Rogers, T. F. *et al.* Isolation of potent SARS-CoV-2 neutralizing antibodies and protection from disease in a small animal model. *Science* **369**, 956-963, doi:10.1126/science.abc7520 (2020).
35 Zost, S. J. *et al.* Potently neutralizing and protective human antibodies against SARS-CoV-2. *Nature* **584**, 443-449, doi:10.1038/s41586-020-2548-6 (2020).
36 Schafer, A. *et al.* Antibody potency, effector function, and combinations in protection and therapy for SARS-CoV-2 infection in vivo. *J Exp Med* **218**, doi:10.1084/jem.20201993 (2021).

37 Mendoza, P. *et al.* Combination therapy with anti-HIV-1 antibodies maintains viral suppression. *Nature* **561**, 479-484, doi:10.1038/s41586-018-0531-2 (2018).

38 Bar-On, Y. *et al.* Safety and antiviral activity of combination HIV-1 broadly neutralizing antibodies in viremic individuals. *Nat Med* **24**, 1701-1707, doi:10.1038/s41591-018-0186-4 (2018).

39 Li, Q. *et al.* The Impact of Mutations in SARS-CoV-2 Spike on Viral Infectivity and Antigenicity. *Cell* **182**, 1284-1294 e1289, doi:10.1016/j.cell.2020.07.012 (2020).

40 Eguia, R. *et al.* A human coronavirus evolves antigenically to escape antibody immunity. *bioRxiv* **5**, 52-28, doi:10.1101/2020.12.17.423313 (2020).

41 Amanat, F. *et al.* A serological assay to detect SARS-CoV-2 seroconversion in humans. *Nat Med* **26**, 1033-1036, doi:10.1038/s41591-020-0913-5 (2020).

42 Grifoni, A. *et al.* Targets of T Cell Responses to SARS-CoV-2 Coronavirus in Humans with COVID-19 Disease and Unexposed Individuals. *Cell* **181**, 1489-1501 e1415, doi:10.1016/j.cell.2020.05.015 (2020).

43 Cohen, A. A. *et al.* Mosaic nanoparticles elicit cross-reactive immune responses to zoonotic coronaviruses in mice. *Science*, doi:10.1126/science.abf6840 (2021).

44 Mastronarde, D. N. Automated electron microscope tomography using robust prediction of specimen movements. *J Struct Biol* **152**, 36-51, doi:10.1016/j.jsb.2005.07.007 (2005).

45 Punjani, A., Rubinstein, J. L., Fleet, D. J. & Brubaker, M. A. cryoSPARC: algorithms for rapid unsupervised cryo-EM structure determination. *Nat Methods* **14**, 290-296, doi:10.1038/nmeth.4169 (2017).

46 Goddard, T. D. *et al.* UCSF ChimeraX: Meeting modern challenges in visualization and analysis. *Protein Sci* **27**, 14-25, doi:10.1002/pro.3235 (2018).

47 Terwilliger, T. C., Adams, P. D., Afonine, P. V. & Sobolev, O. V. A fully automatic method yielding initial models from high-resolution cryo-electron microscopy maps. *Nat Methods* **15**, 905-908, doi:10.1038/s41592-018-0173-1 (2018).

48 Emsley, P., Lohkamp, B., Scott, W. G. & Cowtan, K. Features and development of Coot. *Acta Crystallogr D Biol Crystallogr* **66**, 486-501, doi:10.1107/S0907444910007493 (2010).

49 Gupta, N. T. *et al.* Change-O: a toolkit for analyzing large-scale B cell immunoglobulin repertoire sequencing data. *Bioinformatics* **31**, 3356-3358, doi:10.1093/bioinformatics/btv359 (2015).

50 Soto, C. *et al.* High frequency of shared clonotypes in human B cell receptor repertoires. *Nature* **566**, 398-402, doi:10.1038/s41586-019-0934-8 (2019).

51 Guo, Y., Chen, K., Kwong, P. D., Shapiro, L. & Sheng, Z. cAb-Rep: A Database of Curated Antibody Repertoires for Exploring Antibody Diversity and Predicting Antibody Prevalence. *Front Immunol* **10**, 2365, doi:10.3389/fimmu.2019.02365 (2019).

52 Kyte, J. & Doolittle, R. F. A simple method for displaying the hydropathic character of a protein. *J Mol Biol* **157**, 105-132, doi:10.1016/0022-2836(82)90515-0 (1982).

53 Guy, H. R. Amino acid side-chain partition energies and distribution of residues in soluble proteins. *Biophys J* **47**, 61-70, doi:10.1016/S0006-3495(85)83877-7 (1985).

54 DeWitt, W. S. *et al.* A Public Database of Memory and Naive B-Cell Receptor Sequences. *PLoS One* **11**, e0160853, doi:10.1371/journal.pone.0160853 (2016).

55 Rubelt, F. *et al.* Onset of immune senescence defined by unbiased pyrosequencing of human immunoglobulin mRNA repertoires. *PLoS One* **7**, e49774, doi:10.1371/journal.pone.0049774 (2012).

822